COMPUTER-AIDED CONSTRUCTION OF COMBUSTION CHEMISTRY MODELS

Oleg A. Mazyar, David M. Matheu, Douglas A. Schwer, and William H. Green, Jr.

Department of Chemical Engineering, Massachusetts Institute of Technology, 77 Massachusetts Ave., Cambridge, MA 02139

KEYWORDS: Chemical kinetic models, pressure-dependent rate constants, adaptive chemistry

Introduction

The combustion, oxidation and pyrolysis chemistry of even simple light hydrocarbons can be extremely complex, involving hundreds or thousands of kinetically significant species. Even relatively minor species can play an important role in the formation of undesirable emissions and byproducts. Recently, a number of researchers [1-8] have recognized that the most reasonable way to deal with this complexity is to use a computer not only to numerically solve the kinetic model, but also to construct the model in the first place. We are developing the methods needed to make this feasible, particularly focusing on the need for reliable computer estimates of the pressure-dependent rate constants, rate constants of the reactions with large stereoelectronic effects, and methods for handling situations where the reaction conditions change significantly with time or with spatial position.

We previously devised [8] the first general algorithm for constructing kinetic models appropriate to particular reaction conditions, by numerically testing whether particular species are significant under those conditions. This algorithm can very rapidly and reliably construct rather complex kinetic schemes, testing hundreds of thousands for reactions to find the smaller set which is actually important. It is much less prone to inadvertently omitting an important reaction than other model construction techniques. It has the advantage of clarifying the relationship between the reaction conditions and the kinetic model required. Unfortunately, the existing algorithm is explicitly designed for perfectly mixed, isothermal, isobaric simulations. Relaxing these restrictions raises a number of issues.

Results and Discussion:

A priory rates for combustion reactions

The key issue in constructing any kinetic model, of course, is how to reliably estimate the rate constants required. Many of the important rates for light alkane combustion are known experimentally, though usually over a restricted range of temperatures and pressures (e.g. at room temperature, atmospheric or sub-atmospheric pressure). The highly non-linear combustion process typically involves hundreds of kinetically significant reactive intermediates and even more reactions; it seems unlikely that all the rate constants needed to describe these systems will ever be measured experimentally. What is needed are reliable methods for estimating these reaction rates *a priory*.

Although transition state theory (TST) was proposed more than 60 years ago, and the debate about its microcanonical quantum version known as RRKM has sparked a tremendous amount of effort since the 1960's, this theory was still controversial into the 1990's. It was only over the last decade that conclusive experiments and the elucidation of the connection between TST and quantum scattering decisively established that TST/RRKM is the correct way to calculate most reaction rates. [9-11] Recent advances in computer power and quantum chemistry algorithms have now made it possible to calculate single points on molecular potential energy surfaces (PES's) with something close to "chemical accuracy" of 1-2 kcal/mol. In addition, current DFT technology allows one to calculate rather extensive portions of the PES for even fairly large molecules, albeit with somewhat lower accuracy. [12,13] Several research groups have combined modern quantum chemistry and TST techniques to make *a priory* rate predictions; recent results look very promising. [9,14,15] We have found that in many cases the largest error in *ab initio* rate estimates comes from errors in the calculated barrier height, so one should use high levels of theory for calculating it, but apparently lower levels of theory suffice for estimating the entropic Arrhenius "A" factor (which may be T-dependent).This allows rather accurate rate extrapolations to different temperatures. With some care, complexities such as tunneling, isotope effects, and the large amplitude motions in floppy transition states (TS's) can be modeled accurately *a priory*. [9,14].

Typically rate estimates are made for whole reaction families rather than for individual reactions, an extremely important simplification. The idea is that reaction rates are determined by the functional groups directly involved; the rest of the molecule is more or less a spectator. For example, one would expect that the reactivity of octyl amine and hexyl amine would be very

similar. Usually there are insufficient data to directly verify whether the reaction family idea is valid; but for functional group ideas to work at all it must be at least approximately correct. (For a rare experimental verification see ref. 16).

The Hammond postulate indicates that within a reaction family, the reaction barrier and TS properties should shift with the heat of reaction. These shifts are typically modeled by assuming that the rates follow the simple Arrhenius formula $k(T) = A \exp(-E_a/RT)$, and making linear interpolations between reactions with experimentally determined E_a's (these interpolations are called "Evans-Polanyi", 'LFER", or "Semenov" relations). It is known that the true relationship cannot be linear. Denisov has recently proposed a type of parabolic interpolation. [17] Unfortunately, the experimental data required to make either of these interpolations are often unavailable for the systems of greatest current interest, including many of the reactions important in combustion.

Quantum-chemistry based TST calculations could provide the missing data, but the most accurate quantum techniques are so computationally demanding that only single-point (i.e. fixed geometry) energy calculations are feasible. Much cheaper methods are needed to map out the PES and to determine the vibrational frequencies, etc. required for a TST rate calculations. The method of choice is DFT, which is computationally inexpensive but still fairly accurate in most cases. Unfortunately, current DFT functionals are not reliably enough to be really useful for quantitative kinetics. Current DFT functionals are particularly poor for free-radical oxidations, since they seriously underpredict the strength of peroxidic O-H bonds. [15] We recently developed a method for systematically improving DFT functionals, using as input the results of high-accuracy quantum chemistry calculations. [18] Our approach is based on the fact that the DFT functional determines the electron density as well as the energy; so high-accuracy electron densities provide a strong and very useful constraint on trial functionals.

Many of the components required to make accurate predictions of the chemical kinetics of technologically important processes like combustion already exist. Development and validation of reliable, systematic, quantum/TST-based rate estimation methods would allow us to finally make quantitative predictions about these important chemical processes.

Estimation of pressure-dependent rate constants

For many reactions, pressure-dependent fall-off and chemical-activation effects are very significant. In many cases of importance in combustion chemistry, the initial complex is formed very highly excited, and chemically-activated channels dominate over the thermal pathways. We are currently automating the process of computing pressure-dependent rate constants, so that the computer can do this "on-the-fly" as it constructs the kinetic model. We have devised a general algorithm which constructs every chemically-activated and stabilization reaction pathway, and so can construct and solve the equations which describe the pressure dependence. The required $k(E)$'s and $\rho(E)$'s can be obtained from the high-pressure limit $k(T)$'s and the group-additivity heat capacities by the inverse Laplace transform technique [19] and the "3-frequency" technique [20] respectively. The pressure dependence can be estimated in many different ways ranging from simple approximations to full-blown time-dependent master equations; we will explore the tradeoffs between accuracy and computational speed.

At least initially, we will use the exponential-down model for energy transfer, and the corresponding Troe $\beta k_s[M]$ approximation.[21] For chemically-activated reactions of large molecules, there are a very large number of possible reaction pathways, and some pruning will be necessary. This can be done by setting a criterion for kinetic significance which suppresses the most minor channels. Once one has constructed the pressure-dependence model, it can be solved for a range of pressure and for different initial energy distributions of the activated complex (corresponding to different entrance channels and temperatures). We will test this new tool by computing the pressure dependence of a large number of reactions; in addition to validating the method we expect to find some surprises.

Adaptive complex chemistry for reacting flows

In combustion, the overall rate of reaction is usually controlled as much by mixing as by any rate constant. Conventional reacting-flow simulation techniques can only be used if the chemistry model is very small, since they typically attempt to solve for the concentration of every chemical species in the model at every spatial position at every time point in the simulation. Since the computer can rapidly construct kinetic models adapted to each reaction condition, it should be possible to construct an "adaptive chemistry" reacting flow simulation, where different truncated kinetic models are used at different spatial positions and times. This could dramatically reduce the number of equations which must be solved in the simulation. As a first step towards developing such a simulation, we have been examining how one could in practice develop truncated kinetic schemes known to be reliable over a specific range of reaction conditions. We

will also devise methods for dealing with boundaries between finite elements with different kinetic schemes (involving different numbers of species). For the numerical solution, we will draw heavily on numerical methods for solving differential-algebraic equations with discrete control variables recently developed at MIT. [22] Initially, we will construct the reacting flow simulations by hand, for very simple geometries. Once we demonstrate that the "adaptive chemistry" approach provides a significant advantage over current approaches, we can begin to incorporate the technology developed by others for adaptive gridding [23] that would be required for reacting flows through complex geometries.

References

1. L. Haux, P.-Y. Cunin, M. Griffiths, and G.-M. Come, *J. Chim. Phys.* **1988**, *85*, 739.
2. S.J. Chinnick, D.L. Baulch, and P.B. Ayscough, *Chemom. Itell. Lab. Syst.* **1988**, *5*, 39.
3. E. Ranzi, A. Sogaro, P. Gaffuri, G. Pennati, C.K. Westbrook, and W.J. Pitz, *Combust. Flame* **1994**, *99*, 210.
4. E.S. Blurock, *J. Chem. Inf. Comput. Sci.* **1995**, *35*, 607.
5. L.J. Broadbelt, S.M. Stark, and M.T. Klein, *Comput. Chem. Eng.* **1996**, *20*, 113.
6. M. Nehse, J. Warnatz, and C. Chevalier, *Twenty-Sixth Symposium (International) on Combustion* (The Combustion Institute: Pittsburgh, **1997**).
7. D.J. Klinke and L.J. Broadbelt, *A.I.Ch.E. J.* **1997**, *43*,1828.
8. R.G. Susnow, A.M. Dean, W.H. Green, P. Peczak, & L.J. Broadbelt, *J. Phys. Chem. A* **1997**, *101*, 3731.
9. D.G. Truhlar, B.C. Garrett, and S.J. Klippenstein, *J. Phys. Chem.* **1996**, *100*, 12771.
10. W.H. Miller, *Acc. Chem. Res.* **1993**, *26*, 174.
11. W.H. Green, C.B. Moore, and W.F. Polik, *Ann. Rev. Phys. Chem.* **1992**, *43*, 591.
12. L.A. Curtiss, K. Raghavachari, G.W. Trucks, and J.A. Pople, *J. Chem. Phys.* **1991**, *94*, 7221.
13. A.D. Becke, *J. Chem. Phys.* **1992**, *96*, 2155.
14. See for example (a) S.J. Klippenstein and W.D. Allen, *Ber. Bunsenges. Phys. Chem.* **1997**, *101*, 423; (b) S.J. Klippenstein, A.L.L. East, and W.D. Allen, *J. Chem. Phys.* **1994**, *101*, 9198.
15. W.H. Green, *Int. J. Quantum Chem.* **1994**, *52*, 837.
16. J.B. Koffend and N. Cohen, *Int. J. Chem. Kinet.* **1996**, *28*, 79.
17. E.T. Denisov, *Mendeleev Commun.* **1992.**
18. D.J. Tozer, N.C. Handy, and W.H. Green, *Chem. Phys. Lett.* **1997**, *273*, 183.
19. W. Forst, *J. Phys. Chem.* **1972**, *76*, 342.
20. J.W. Bozzelli, A.Y. Chang, and A.M. Dean, *Int. J. Chem. Kinet.* **1997**, *29*, 161.
21. R.G. Gilbert, K. Luther, and J. Troe, *Ber. Bunsenges. Phys. Chem.* **1983**, *87*, 169.
22. T. Park and P.I. Barton, *ACM Trans. Mod. Computer Sim.* **1996**, *6*, 137.
23. B.A.V. Bennett and M.D. Smooke, *J. Comp. Phys.* **1999**, *151*, 684.

KINETIC MODELING OF THE FORMATION OF POLYCYCLIC AROMATIC HYDROCARBONS

Henning Richter, Timothy G. Benish, Francisco Ayala and Jack B. Howard

Department of Chemical Engineering, Massachusetts Institute of Technology, 77 Massachusetts Avenue, Cambridge, MA 02139-4307, U.S.A.

Keywords: Combustion, PAH, Kinetics

1. INTRODUCTION

Growing evidence of the significant role of polycyclic aromatic hydrocarbons (PAH) in the formation of small particles such as soot in atmospheric aerosols and the known mutagenic or tumorigenic properties of at least some of them[1,2] necessitate a better understanding of the chemical growth process leading to larger and larger molecules. Combustion represents a major source of PAH and soot particles in the environment, therefore more efficient and cleaner combustion processes would lead to a significant reduction of pollution and to a more economic use of fossil fuels. Kinetic modeling can be expected to be a powerful tool for a better understanding of chemical processes responsible for PAH and utimately soot formation. A sufficiently developed model will finally allow the assessment of optimized operating conditions for practical combustion devices. In the recent years detailed kinetic models describing the formation of small and medium PAH have been developed and tested against experimental data obtained under well defined laboratory conditions such as shock tube pyrolysis[3,4] or premixed flames[5-11].

In the present work, two sets of experimental data obtained with different laboratory combustors, fuels and pressures are used in order to improve the reliability and in particular the detailed understanding of elementary reaction steps of a kinetic model developed recently for fuel rich benzene combustion under low pressure conditions[11].

2. APPROACH

A nearly sooting low pressure premixed, laminar, one-dimensional benzene/oxygen/argon flame (equivalence ratio ϕ= 1.8, 30% argon, 50 cm s^{-1}, 2.67 kPa) for which large sets of experimental data[12,13] are available was modeled using the Premix code[14]. This flame has been studied by Bittner and Howard[12] using molecular beam sampling coupled to mass spectrometry (MBMS) to establish concentration profiles for stable species up to 202 amu and radicals up to 91 amu. The temperature profile was determined with a thermocouple taking into account heat losses by radiation. Because the measurements include unstable, often radical, intermediates the data provide valuable insights and have been used for different modeling studies focusing on a better understanding of benzene oxidation chemistry[5,6,9] and for the assessment of the first reaction steps of PAH growth[11]. The use of nozzle beam sampling followed by radical scavenging and subsequent analysis by gas chromatography coupled to mass sepctrometry, a technique developed and sucessfully used by Hausmann et al.[15], allowed Benish[13] to extend the data set to species up to 276 amu in the case of stable species and up 201 amu for radicals.

The other experimental data used in the present work consist of concentration profiles of light gas species and PAH up to 300 amu measured for fuel rich $C_2H_4/O_2/N_2$ combustion (ϕ= 2.2) in a jet-stirred-reactor/plug-flow reactor (JSR/PSR) system by means of gas chromatography operating at amospheric pressure[16,17]. The temperature was constant at 1630K in the JSR and 1630 K in the PFR. The outlet of the JSR was coupled to the inlet of the PFR. Kinetic models can be applied easily to both JSR and PFR which allows the comparison of model predictions to experimental data.

The parallel investigation of PAH formation under different conditions at low pressure, atmospheric pressure and different fuels, i. e., benzene and ethylene, is particularly challenging for a kinetic model. The present study is based on a recently published model tested for low pressure conditions[11] but with the rate constants of pressure-dependent chemically activated reactions, e. g., for benzene formation via the reaction of acetylene with 1-butadienyl radical[20], which have been systematically adapted to 1 atm using the QRRK (Quantum Rice-Ramsperger-Kassel) technique[21]. Thermodynamic data have been critically assessed and updated with available literature data or, in the case of poorly known PAH radicals, computed using *ab initio* techniques. Vibrational analysis performed on the optimized geometries allowed the determination of entropies and heat capacities while enthalpies of formation were determined by means of isodesmic reactions. Rate constants of reactions involved in the growth process have been investigated. The potential energy surfaces, including transition states, of the reactions phenyl + acetylene and of 1-naphthyl + acetylene have been explored. The resulting high pressure rate constants for the different elementary reactions followed by a QRRK treatement allowed the determination of "apparent" rate constants at different pressures and temperatures

describing the competing pathways. In the case of the reaction of 1-naphthyl with acetylene, as shown in Fig. 1, rate constants for the formation of 1-vinylnaphthalene, 1-naptththylacetylene and acenaphtalene were determined and implemented in the kinetic model.

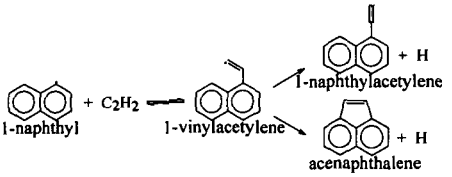

Fig. 1. Reaction pathways of 1-naphthyl + acetylene

3. RESULTS

a) Fuel Consumption and Formation of Main Products and Intermediates

A meaningful testing of a chemical reaction mechanism describing the growth of polycyclic aromatic hydrocarbons requires the correct prediction of key species which intervene in this process. The previously published kinetic model[11] showed good prediction capabilities for key products but also intermediate radicals such as *H* or *OH* compared to the MBMS data measured by Bittner and Howard[12]. In addition, the reliability of the model has been confirmed by means of the comparison of its predictions with experimental mole fraction profiles of stable species in a sooting low pressure premixed benzene/oxygen/argon flame (ϕ= 2.4, 5.33 kPa)[22]. However, an underprediction by a factor of ≈2.5 of the the peak mole fraction of acetylene was observed in the nearly sooting benzene flame studied in the present work while peak values of cyclopentadienyl (C_5H_5) and phenyl (C_6H_5) showed corresponding overpredictions[11]. A significant improvement of the predictions of these three species could be achieved by the addition of the oxidation of phenyl and phenoxy radicals to benzoquinone as suggested by Frank et al.[23] followed by the unimolecular decay and oxidation of benzoquinone to different C_6 and C_5 species leading ultimately to acetylene as discussed by Alzueta et al.[24]. Fig. 2 shows the predictions of the model developed in the present work for cyclopentadienyl and acetylene in comparison to the data of Bittner and Howard[11]. For the same flame, predictions and experimental data for benzene comsumption, CO_2 and water formation as well as the experimental temperature profile used for the model computation are summarized in Fig. 3. Also the update of the thermodynamic database, described above, contributed significantly to the improvement of the agreement between model predictions and experimental data.

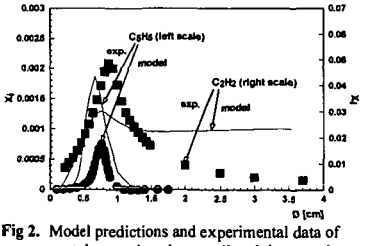

Fig 2. Model predictions and experimental data of acetylene and cyclopentadienyl in a nearly sooting premixed benzene/oxygen/argon flame (ϕ= 1.8, 2.67 kPa)[11].

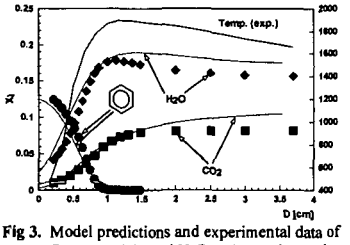

Fig 3. Model predictions and experimental data of Benzene, CO_2 and H_2O and experimental temperature profile in a nearly sooting premixed benzene/oxygen/argon flame (ϕ= 1.8, 2.67 kPa)[11].

A similar approach has been taken in order to check the prediction capability of the atmospheric pressure version of the model using ethylene combustion data from the JSR/PFR system operating at amospheric pressure[16,17]. The performance of the model was first tested for the comsumption of the reactant and the formation of key products and intermediates. Fig. 4 and 5 show the results of the model for ethylene, acetylene, H_2 and CO_2 in comparison with experimental data measured in the PFR at 1620K. In particular the excellent prediction of acetylene, a species assumed to be a key species in the formation proccss of PAH, is essential for the quality of the model but also the good agreements for ethylene consumption and CO_2 formation, representing the reactant and one of the main products, is encouraging. H_2 is only slightly underpredicted, another important finding because of the importance of hydrogen-abstraction reactions (R-H + H ↔ R• + H_2) in the PAH growth process which may be affected by the location of the equilibrium on the reaction coordinate and therefore by the concentration of molecular hydrogen. Unfortunately, no experimental data on atomic hydrogen and other radical species are available due to the sampling technique used for the jet-stirred/plug-flow reactor system so that no check of equilibria exclusively based on experimental data has been possible.

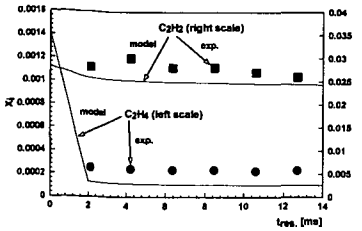

Fig 4. Model predictions and experimental data of ethylene and acetylene in a plug-flow reactor at 1620 K and 1 atm; JSR: C_2H_4/ O_2/N_2 (ϕ= 2.2, 71.6% N_2, 1630K)[16,17].

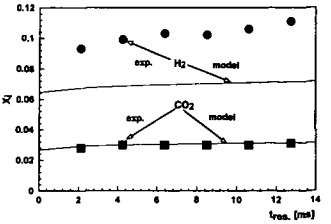

Fig 5. Model predictions and experimental data of H_2 and CO_2 in a plug-flow reactor at 1620 K and 1 atm; JSR: $C_2H_4/O_2/N_2$ (ϕ= 2.2, 71.6% N_2, 1630 K, 1 atm)[16,17].

b) Beginning of the Growth Process

The formation of polycyclic aromatic hydrocarbons (PAH) and of soot depends mainly on the the initial relative concentration of fuel and oxidizer, i. e., the equivalence ratio, reflecting the competition of oxidation with growth reactions. The latter becomes more favorable with increasing equivalence ratio. Assuming an essential role of a subsequent growth process from small to larger and larger PAH, the formation of the first aromatic species is of great interest. The importance of the formation of the first aromatic ring is confirmed by the order of the sooting tendencies: naphthalenes > benzenes > diolefins > monoolefins > paraffins[25]. Because of the presence of the first aromatic ring in the initial fresh gas mixture in the case of benzene combustion, the formation pathways for benzene will be discussed for ethylene combustion in the jet-stirred/plug-flow reactor system. Different pathways leading to the first aromatic ring, i. e., benzene or phenyl, have been discussed in the past[26] and are implemented in the present model. The analysis of the rates of production in the present work showed the reaction between two propargyl (C_3H_3) being the dominant pathway but also the reaction of acetylene with a vinylacetylene radical (HCCHCCH) and of allene (CH_2CCH_2) with a C_3H_2 radical contributed significantly. It should be pointed out that no general conclusions can be drawn from these results because of the likely strong dependence of the relative contributions of the different pathways on experimental conditions such as temperature or fuel type. Nevertheless, the use of different pathways described previously in the literature in the present model allows an at least satisfactory agreement with experimental data as shown in Fig. 6.

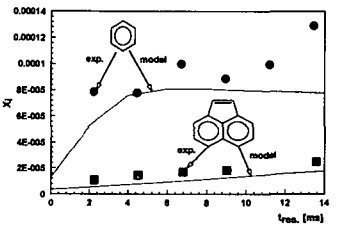

Fig 6. Model predictions and experimental data of benzene and acenaphthalene in a plug-flow reactor at 1620 K and 1 atm; JSR: C_2H_4/ O_2/N_2 (ϕ= 2.2, 71.6% N_2, 1 atm)[16,17].

c) Formation of the Second Aromatic Ring

Beginning with the first aromatic ring, mainly two pathways may lead to the formation of the next larger fused PAH, naphthalene. First, two subsequent H-abstraction/acetylene-addition steps[3,10] can lead to 1-naphthyl radicals, stabilized in the next step by recombination with atomic hydrogen. The other possibility consists of the reaction of two cyclopentadienyl radicals[7,11,27,28]. The contribution of different pathways to the rate of formation of cyclopentadienyl radicals has been checked in the jet-stirred reactor and unimolecular decay of phenoxy was shown to be dominant. Napthalene formation has been investigated in both systems studied in the present work. A significant underprediction by a factor of ≈3 (not shown) was observed for the JSR/PFR system; the analysis of the rate of production revealed that nearly all naphthalene was formed via the hydrogen-abstraction/acetylene-addition pathway starting with benzene while no significant contribution of cyclopentadienyl radicals could be observed. A totally different picture was observed for the nearly sooting low pressure premixed benzene flame. Confirming prior results[7,8,11], naphthalene formation is dominated by the reaction between two cyclopentadienyl moities. The comparison of the model prediction with the experimental naphthalene profile measured by Benish shows an excellent agreement (Fig. 7).

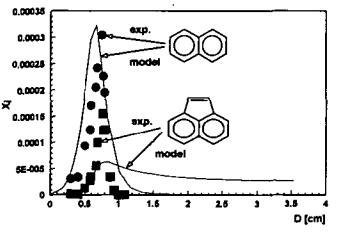

Fig 7. Model predictions and experimental data of naphthalene and acenaphthalene in a nearly sooting premixed benzene/oxygen/ argon flame (ϕ= 1.8, 2.67 kPa)[13].

Recent measurements of radical concentration profiles in the benzene flame studied in this work[13] allowed the assessment of the role of hydrogen-abstraction/acetylene-addition pathway under the condition of this flame. In fact, the reaction of the phenylacetylene radical with acetylene to 1-napthyl (Fig. 8), represents the limiting step for the formation of 1-naphthyl. In contradiction to the good agreement observed for 2-naphthyl radicals (Fig. 10), the 1-naphthyl peak concentration is significantly underpredicted (Fig. 9). As shown in in Fig. 9, the total removal of the hydrogen-abstraction /acetylene addition pathway (Fig. 8) leads to a drastic increase of the 1-naphthyl peak mole fraction, in agreement with the experimental data, while a lack of sufficient consumption in the burnt gases is observed. Based on this observation, completed by tests of the impact of slight adjustments of thermodynamic and kinetic data, it seems likely that the 1-napthyl concentration, at least under the present conditions, is mainly governed by the equilibrium of the ring closure reaction (Fig. 8). Also the drastic decrease of the 1-naphthyl mole fraction at the end of the flame front seems to be strongly influenced by the reverse reaction (Fig. 9). Therefore, uncertainteties on thermodynamic and kinetic data may be responsible for the underprediction of 1-naphthyl. This hypothesis is consistent with a much better agreement between the model prediction for the 2-naphthyl radical and the corresponding experimental profile (Fig. 10). 2-naphthyl is formed by hydrogen abstraction from naphthalene and is not directly involved in the above mentioned equilibrium.

Fig 8. Napthalene formation via the hydrogen-abstraction/acetylene addition pathway.

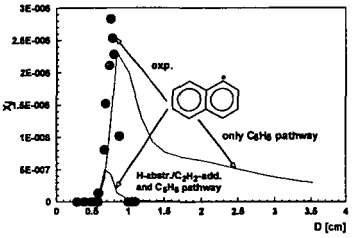

Fig 9. Model predictions and experimental data of 1-naphthyl in a nearly sooting premixed benzene/oxygen/argon flame (ϕ= 1.8, 2.67 kPa)[13]; use of complete model and after removal of H-abstraction/C_2H_2-addition pathway.

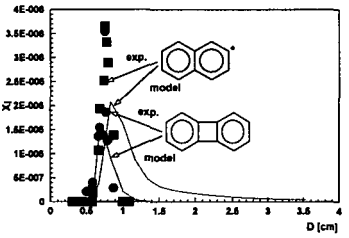

Fig 10. Model predictions and experimental data of 2-naphthyl and biphenylene in a nearly sooting premixed benzene/oxygen/argon flame (ϕ= 1.8, 2.67 kPa)[13].

d) Further Growth Process

Acenaphthalene, a PAH containing a five-membered ring, is usually an abundant species in the exhaust of combustion systems generating PAH. The comparison of model prediction with experimental data is shown for ethylene combustion in the JSR/PFR system (Fig. 6) as well as for low pressure benzene combustion (Fig. 7). A particular good agreement could be achieved in the JSR/PFR system, nethertheless also the significant underproduction of naphthalene in this system must be taken into account which leads to the assumption of an even too pronounced acenapthalene formation. The analysis of the net production rate of acenaphthalene shows a nearly exclusive formation via the reaction of acetylene with 1-naphthyl (Fig. 1), using the rate constant determined for 1 atm by means of the QRRK approach discussed above. A different situation has been observed in the case of low pressure premixed benzene combustion, in agreement with prior work[11], where the exclusive use of the reaction between 1-naphthyl and acetylene yields an underprediction of at least 20-fold. This finding confirms the conclusion of Hausmann et al.[15] that another, yet unknown, acenapthalene formation pathway exists. In the present work an additional acenaphthalene pathway has been suggested and implemented in the model. The isomerization of a biphenylene radical followed by hydrogen loss to acenaphthalene has been assumed and led to a significant improvement in the predictions of acenaphthalene but also biphenylene (Fig. 10), both of which species were measured by Benish[13]:

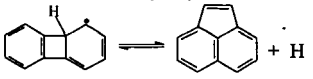

4. CONCLUSIONS

In conclusion, it can be stated that the kinetic model developed in the present work shows at least encouraging prediction capabilities for the first steps in the growth process to larger and larger polycyclic aromatic hydrocarbons. In particular, its satisfactory performance for two

different fuels and pressures increases its value for potential practical application. In next steps, the model will be extended to larger PAH, including up to eight aromatic rings, and a soot formation model will be implemented.

Acknowledgments

We are grateful to the Division of Chemical Sciences, Office of Basic Energy Sciences, Office of Energy Research, U.S. Department of Energy, under Grant No. DE-FG02-84ER13282 for financial support of the research. The authors thank Prof. J. W. Bozzelli from the New Jersey Institute of Technology for providing software and valuable advice. Prof. W. H. Green and Dr. O. A. Mazyar from MIT are acknowledged for their contributions to the computational determinatation of kinetic and thermodynamic data as well as for many helpful discussions.

References

(1) Durant, J. L.; Busby, W. F.; Lafleur, A. L.; Penman, B. W.; Crespi, C. L. Mutation Research **1996**, 371, 123.
(2) Denissenko, M. F.; Pao, A.; Tang, M.; Pfeifer, G. P. Science **1996**, 274, 430.
(3) Frenklach, M.; Clary, D. W.; Gardincr, W. C.; Stein, S. E. Twentieth Symposium (International) on Combustion; The Combustion Institute: Pittsburgh, PA, 1984; p 887.
(4) Colket, M. B.; Seery, D. J. Twenty-Fifth Symposium (International) on Combustion; The Combustion Institute: Pittsburgh, PA, 1994; p. 883.
(5) Lindstedt, R. P.; Skevis, G. Combust. Flame **1994**, 99, 551.
(6) Zhang, H.-Y.; McKinnon, J. Th. Combust. Sci. and Tech. **1995**, 107, 261.
(7) Marinov, N. M.; Pitz, W. J.; Westbrook, C. K.; Castaldi, M. J.; Senkan, S. M. Combust. Sci. and Tech. **1996**, 116-117, 211.
(8) Castaldi, M. J.; Marinov, N. M.; Melius, C. F.; Huang, J.; Senkan, S. M.; Pitz, W. J.; Westbrook, C. K. Twenty-Sixth Symposium (International) on Combustion; The Combustion Institute: Pittsburgh, PA, 1996; p. 693.
(9) Tan, F.; Frank, P., Twenty-Sixth Symposium (International) on Combustion; The Combustion Institute: Pittsburgh, PA, 1996; p. 677.
(10) Wang, H.; Frenklach, M. Combust. Flame **1997**, 110, 173.
(11) Richter, H.; Grieco, W. J.; Howard, J. B. Combust. Flame **1999**, 119, 1.
(12) Bittner, J. D.; Howard, J. B. Eighteenth Symposium (International) on Combustion; The Combustion Institute: Pittsburgh, PA, 1981; p 1105.
(13) Benish, T. G. Ph.D. Thesis, Department of Chemical Engineering, Massachusetts Institute of Technology **1999**, Cambridge, MA, USA.
(14) Kee, R. J.; Grcar, J. F.; Smooke, M. D.; Miller, J. A. (1997). *A FORTRAN Program for Modeling Steady Laminar One-Dimensional Premixed Flames*. Sandia Rept. SAND85-8240.
(15) Hausmann, M.; Hebgen, P.; Homann, K.-H. Twenty-Fourth Symposium (International) on Combustion, The Combustion Institute: Pittsburgh, PA, 1992; p. 793.
(16) Marr, J.A.; Giovane, L. M.; Longwell, J. P.; Howard, J. B.; Lafleur, A. L. Combust. Sci. and Tech. **1994**, 101, 301.
(17) Marr, J. A. Ph.D. Thesis, Department of Chemical Engineering, Massachusetts Institute of Technology **1993**, Cambridge, MA, USA.
(18) Glarborg, P.; Kee, R. J.; Grcar, J. F.; Miller, J. A. (1986). PSR: *A FORTRAN Program for Modeling Well-Stirred Reactors*. Sandia Rept. SAND86-8209.
(19) Lutz, A. E.; Kee, R. J.; Miller, J. A. (1997). SENKIN: *A FORTRAN Program for Predicting Homogeneous Gas Phase Chemical Kinetics with Sensitivity Analysis*. Sandia Rept. SAND87-8248.
(20) Westmoreland. P. R.; Dean, A. M.; Howard, J. B.; Longwell, J. P. J. Phys. Chem. **1989**, 93, 8171.
(21) Dean, A. M.; Bozzelli, J. W.; Ritter, E. R. Combust. Sci. and Tech. **1991**, 80, 63.
(22) McKinnon, J. T.; Howard, J. B. Twenty-Fourth Symposium (International) on Combustion, The Combustion Institute: Pittsburgh, PA, 1992; p. 965.
(23) Frank, P.; Herzler, J.; Just, T.; Wahl, C. Twenty-Fifth Symposium (International) on Combustion, The Combustion Institute: Pittsburgh, PA, 1994; p. 833.
(24) Alzueta, M. U.; Oliva, M.; Glarborg, P. Int. J. Chem. Kinet. **1998**, 30, 683.
(25) Palmer, H. B.; Cullis, C. F. The Formation of Carbon from Gases, Chemistry and Physics of Carbon (editor Walker, P. L.), Vol. 1, p. 265. Marcel Dekker, New York, (1965).
(26) Miller, J. A.; Melius, C. F. Combust. Flame **1992**, 91, 21.
(27) Dean, A. M. J. Phys. Chem. **1990**, 94, 1432.
(28) Melius, C. F.; Colvin, M. E.; Marinov, N. M.; Pitz, W. J.; Senkan, S. M. Twenty-Sixth Symposium (International) on Combustion, The Combustion Institute: Pittsburgh, PA, 1996; p. 685.

NUMERICAL MODELING OF NO REDUCTION USING BIOMASS-BASED MATERIALS AS REBURN FUELS

Sumeet Bhalla and Sarma V. Pisupati
Department of Energy and Geo-Environmental Engineering
The Pennsylvania State University
110 Hosler Building
University Park, PA 16802

INTRODUCTION

The role of both homogenous and heterogeneous reactions in use of solid fuels such as coal for NO_x reduction has been discussed in some previous studies [1,2,3,4]. However Wendt [5], and Mereb and Wendt [6] have discounted heterogeneous reactions showing that they have minor contribution towards reburning. The reduction potential of a fuel depends on its ability to produce CH_i radicals to react with NO. Assuming only homogeneous gas phase reactions to participate in reduction, a higher volatile matter content of the fuel will enhance the NO_x reduction. In the recent past, the reburning process is reasonably well understood for use of coal and natural gas as reburn fuels [2, 3, 7, 8, 9, 10,11]. However pyrolysis products of biomass and biomass pyrolysis oils (bio-oils) have also been shown to cause NO_x reduction by mechanisms similar to reburning[12, 13]. Biomass and biomass based products offer the advantage of not only reduced SO_2, NO_x emissions because of low nitrogen and sulfur content but also reduced green house gases (N_2O and CO_2). However some fundamental questions such as the relative importance of homogeneous gas phase reactions in the process still need to be addressed.
In the present study, gas composition from flash pyrolysis of BioLime™ from an earlier study[14] was used to model NO reduction through homogeneous gas phase reactions when BioLime™ is used as a reburn fuel. The numerical predictions were then compared with the NO_x emissions from a down-fired combustor (DFC) to validate the model. A difference in NO_x reduction was observed by using two different BioLime™ samples as reburn fuel under similar operating conditions. This was believed to be due to difference in yield of flash pyrolysis products of the different BioLime™. With this in mind the model was further used to study the relative contribution of each of the pyrolysis gas species in NO reduction through homogeneous reactions. The predictions were then verified by experimental results from the flow reactor.

EXPERIMENTAL

Raw Materials
Two biomass based materials called BioLime™ I and III were obtained from DynaMotive Technologies Corporation. BioLime™ was produced by reacting pyrolysis oils from biomass with air, and lime/water slurry in a stirred. BioLime™ I and III had approximately 7 and 14 wt. % calcium, respectively. Compositional analysis of the samples is shown in Table 1.

	BioLime™ I (As Determined)	BioLime™ III (As Determined)
Carbon (wt. % daf)	48.5	38.7
Hydrogen (wt. % daf)	7.7	8.4
Nitrogen (wt. % daf)	0.23	0.21
Sulfur (wt. % daf)	0.01	0.02
Oxygen (wt. % daf by diff)	43.5	52.6
Ash (wt. % db)	20.9	48.5
Moisture (wt. %)	7.97	4.11

Table 1 Compositional analysis on as determined and dry basis for two BioLime™ samples

Down Fired Combustor
The DFC is 10 ft high with a 20-inch internal diameter rated at a nominal firing rate of 0.5 million Btu/h.. Several 4-inch sampling ports are located along the combustor. Sample ports are numbered 1 through 10 starting at the top. BioLime™ is introduced through port 5 into the reburn zone. The reburn zone parameters are shown in Table 2 . The flue gases from the heat exchanger pass through a pulse jet baghouse for particulate matter collection. The BioLime™ is prepared, stored in a day tank and pumped to the burner by a Moyno™ progressive cavity pump. The gaseous emissions data during the steady state was averaged.

DFC Reburn zone parameters	Values with the units
Diameter	50.8 cm
Total length	96.52 cm
Volume	195600 cm^3
Pressure	1 atm
Residence time	1.127 seconds
Inlet temperature at the center	1415 K
Inlet temperature at the wall	1426 K

Table 2 Down fired combustor reburn zone parameters

Modeling NO_x Reductions

All numerical calculations were done using a PSR computer code[15], which runs in conjunction with the Chemkin library[16]. The reverse rate constants were obtained from the forward rate constants and the thermodynamic data, mainly taken from the Sandia Thermodynamic Database[17]. The code computes species concentrations from the balance between the net rate of production of each species by chemical reaction and the difference between the input and output flow rates of species. The model used to predict NO emissions was taken from the studies of Kilpinen *et al.*[18], Glarborg *et al.*[19], and Prada and Miller[20]. In general the mechanism includes generation of hydrocarbon radicals from C_1 and C_2 parent hydrocarbons, oxidation mechanisms for HCN, and NH_3, together with a subset of the interactions between the hydrocarbon radicals and the nitrogenous species. The nitrogen-hydrocarbon chemistry is essentially an extension of the Miller and Bowman mechanism[21].

The procedure and assumptions in the above study are:

(1) Only homogeneous gas phase reactions are responsible for NO reduction. The effect of heterogeneous reactions is neglected. Gases from pyrolysis of BioLime™ react with NO_x in the reburn zone to form N_2 and nitrogenous intermediate species such as HCN and NH_3.
(2) Gas concentrations are calculated from the yields reported in an earlier study[14].
(3) Reburn fuel is mixed rapidly and perfectly with the products of combustion from the primary zone. This is achieved by use of high-pressure injection nozzle for feeding the reburn fuel.
(4) Reburn fuel is pyrolyzed instantly on entering the combustor and therefore pyrolysis kinetics does not control the NO_x reduction kinetics.
(5) The kinetics of reburning is controlled by the rate constants for the hydrocarbon-NO reaction system. The effect of mass transfer is neglected. This follows from the previous two assumptions.
(6) An average of the wall and bulk temperature at the point of reburn fuel injection is used as the inlet temperature for the calculations.
(7) Gas densities are calculated at the reburn zone inlet temperatures.
(8) The flue gas in reburn zone consists of 14% CO_2, 2.0% O_2, and 497 ppm of CO in nitrogen base. These concentrations of CO_2, O_2, and CO are chosen to be consistent with those of a coal primary flame operated at stoichiometric ratio of 1.0-1.1.
(9) A residence time of 1.127 seconds is used for the calculations, which is consistent with the residence time in reburn zone of the down-fired combustor.

RESULTS AND DISCUSSION

Predictions of NO_x emissions from the model along with the down-fired combustor data are shown in Table 3. The reburn zone stoichiometry was based on the total amount of fuel and oxidizer that entered the down fired combustor in the first two zones of the combustor divided by the stoichiometric requirement for the primary and reburn fuel[9]. The predictions from model match closely with the DFC data. The results showed a higher NO_x reduction for BioLime™ I than III. However, stoichiometry was different for different runs when BioLime™ I and III are used as reburn fuel. Therefore, to further compare the performance of BioLime™ I and III, NO_x reduction was estimated for both BioLime™ for each run. The results are shown in Figure 1. It can be seen that BioLime™ I produced a higher NO_x reduction than BioLime™ III, and is attributed to the higher yield of total pyrolysis gases for BioLime™ I. These results are in agreement with the studies of Kicherer *et. al.* [22], who have shown that the main reduction effect is due to the volatiles of the reburning fuel. Therefore, a higher yield of pyrolysis gases will result in a higher NO_x reduction. Different pyrolysis gases can have different NO_x reduction potential. However as seen from Table 3, the relative percentage of pyrolysis gases added was different for different runs. Knowledge of relative contribution of pyrolysis gases in NO_x reduction would help to choose a biomass feedstock that increases the yield of desired species. With this in mind a parametric analysis is done using the model to study the effect of varying concentration of hydrocarbons, CO_2, CO, H_2.

Run (BioLime™)	Stoichiometry	% of Hydro carbon added	% CO_2 added	% CO added	% H_2 added	% NO_x Reduction (DFC)	% NO_x Reduction (Model)
Run 1(I)	0.501	0.13	14.88	0.25	0.23	17.0	16.0
Run 2(I)	0.517	0.14	14.92	0.26	0.24	16.2	16.8
Run 3(III)	0.549	0.09	14.50	0.18	0.20	13.6	11.2
Run 4(III)	0.652	0.04	14.20	0.10	0.08	11.6	4.4
Run 5(III)	0.656	0.05	14.27	0.12	0.11	12.5	7.2
Run 6(III)	0.717	0.05	14.27	0.12	0.11	12.6	6.3

Table 3. Model predictions for percentage NO_x reduction with NO_x reduction from DFC.

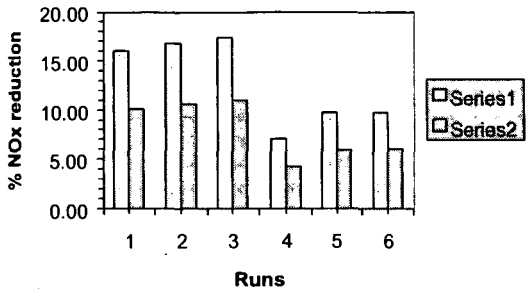

Figure 1. Influence of BioLime™ used on NO_x reduction. The % NO_x reduction is predicted from model for both BioLime™ for each run condition.(Series 1 – BioLime™ I, Series 2 - BioLime™ III)

The results were then verified using the flow reactor. The setup of the flow reactor is discussed in an earlier study[14]. CO_2, CO, and H_2 had very little effect on NO_x reduction. Hydrocarbons were seen to be mainly responsible for causing reduction in emissions of NO_x. Kilpinen *et. al.* [23], Chen *et. al.* [24] , Mereb and Wendt [25] have also shown that for natural gas reburning CO, and H_2 are useable as reburn fuels, even though the rates of reaction for NO reduction by CO and H_2 are significantly slower compared to NO-hydrocarbon reactions. Two main stages are considered to be mainly responsible for nitric oxide reduction. First is the conversion of NO to HCN, through reaction with CH_i and HCCO.

$$NO + HCCO \quad HCNO + H \quad HCN$$
$$NO + CH_2 \quad HCN + OH$$
$$NO + CH_3 \quad H_2CN + M \quad HCN$$
$$NO + CH_3 \quad HCN + H_2O$$

The second stage is the reaction of HCN with the oxidizing species (O, OH) to form NH_i, N_2, and NO. HCN is first converted to isocyanic acid and HNCO primarily by

$$HCN + OH \quad HOCN + H \quad HNCO$$

and to a lesser extent also through the direct reaction

$$HCN + OH \quad HNCO + H$$

The HNCO reacts further to NH_2. This occurs primarily by the reaction with H radical

$$HNCO + H \quad NH_2 + CO$$

The NH_2 radical depending on the conditions can be converted to N_2, NH_3, or NO.

Burch *et. al.* [26] in their study of different fuels (methane, hexane, benzene, and coal) have also shown that NO_x reduction efficiency can also be related to C/H ratio for the fuel. Carbon rich fuels produce more CH_i fragments, leading to a lower NO_x concentration. BioLime™ I had a C/H ratio of 6.3 whereas BioLime™ III had a C/H ratio of 4.6. Therefore, a BioLime™ with a higher C/H ratio will help to increase the NO_x reduction.

CONCLUSIONS

1) Percentage of NO_x reduction using BioLime™ as a reburn fuel was accurately predicted using the homogeneous gas phase reaction model. For most of the conditions, the percentage NO_x reduction predicted from model was well within the allowable variation from the experimental results from down fired combustor and flow reactor. However in some studies like those of Smart and Morgan [27], Chen and Ma [28] have also shown the role of char reactions in NO_x reduction.
2) The higher NO_x reduction potential of BioLime™ I over BioLime™ III was attributed to the higher yield of total pyrolysis gases.
3) The parametric study from flow reactor showed that the CO, CO_2, and H_2 have very little effect and hydrocarbon reactions are mainly responsible for NO_x reduction. Hence a fuel with higher C/H ratio will produce more CH_i fragments, and therefore, result in a better NO_x reduction.

REFERENCES

[1]Chen, W-Y, and Ma, L., "Effect of Heterogeneous Mechanisms During Reburning of Nitrogen Oxide", AIChE Journal, Vol. 42, No. 7, 1996, pp. 1968-1976.

[2] Splicthoff H., Greul U., Rüdiger, H., and Hein, K. R. G., "Basic effects on NO_x emissions in air staging and reburning at a bench-scale test facility", Fuel, Vol. 75, No.5, 1996, pp. 560-564.

[3] Liu, H., Hampartsoumian, E., and Gibbs, B. M., " Evaluation of the optimal fuel characteristics for efficient NO reudtcion by coal reburning", Fuel, Vol. 76, No. 11, 1997, pp. 985-993.

[4] Burch, T. E., Tillman, F. R., Chen, W-Y, and Lester, T. W., Conway, R. B., and Sterling, A. M., "Partitioning of Nitrogenous Species in the Fuel-Rich Stage of Reburning", Energy and Fuels, Vol. 5, No. 2, 1991, pp.231-237.

[5] Wendt, J. O. L., "Mechnism Governing the Formation and Destruction of NO_x and Other Nitrogenous Species in Low NO_x Coal Combustion Systems", Combustion Science and Technology, Vol. 108, 1995, pp. 323-344.

[6] Mereb, J.B., and Wendt J. O. L., "Air staging and reburning mechanisms for NO_x abatement in a laboratory coal combustor", Fuel, Vol. 73, No. 7, 1994, pp. 1020-1026.

[7] Bilbao, R., Millera, A., Alzueta, M. U., "Influence of the Temperature and Oxygen Concentration on NO_x Reduction in the Natural Gas Reburning Process", Industrial Engineering Chemistry, Vol. 33, 1994, pp. 2846-2852.

[8] Ashworth, B., Sommer, T., Moyeda, D., and Payne, R., "Reburning for Utility Boiler NO_x Control A Comparison of Theory and Practice", Joint Power Generation Conference, Vol. 1, ASME, 1996, pp. 67-76.

[9] Smart, J. P., and Morgan, D. J., "The effectiveness of multi-fuel reburning in an internally fuel-staged burner for NO_x reduction", Fuel, Vol. 73, No. 9, 1994, pp. 1437-1442.

[10] Kicherer, A., Splicthoff, H., Maier, H., and Hein, K. R. G., " The effect of different reburning fuels on NO_x-reduction," Fuel, Vol. 73, No. 9, 1994, pp. 1443-1446.

[11] Burch, T. E., Tillman, F. R., Chen, W-Y, and Lester, T. W., Conway, R. B., and Sterling, A. M., "Partitioning of Nitrogenous Species in the Fuel-Rich Stage of Reburning", Energy and Fuels, Vol. 5, No. 2, 1991, pp.231-237.

[12] Rüdiger, H., Greul, U., Splicthoff, H., and Hein, K. R. G., "Distribution of fuel nitrogen in pyrolysis products used for reburning", Fuel, Vol. 76, No. 3, 1997, pp. 201-205.

[13] Pisupati, S. V., Simons, G. A., Oehr, K. H., and Zhou, J., "Effect of BioLime™ Atomization Characteristics on Simultaneous NO_x and SO_2 Capture in Coal Combustion Systems", International Pittsburgh Coal Conference, 14th, 1997.

[14] Bhalla, S. and Pisupati, S.V., "A Study of Composition and Pyrolysis Behavior of Biomass-Based Materials for NO_x Reduction" Proceedings of The Sixteenth Annual International Pittsburgh Coal Conference, October 11-15, 1999 Pittsburgh, University of Pittsburgh, CD-ROM Paper No. 15-3, 1999

[15] Glarborg, P., Kee, R. J., Grear, J. F., and Miller, J. A., "PSR: A Fortran Program for

Modeling Well-Stirred Reactors", SAND86-8209.UC-4 (1992a), Sandia National Laboratories, Livermore, CA, 1989

[16] Kee, R J., Rupley, F. M., and Miller, J. A., "Chemkin II: A Fortran Chemical Kinetics Package for the Analysis of Gas-Phase Chemical Kinetics", SAND87-8215, Sandia National Laboratories, Livermore, California, 1989.

[17] Kee, R. J., Rupley, F. M., and Miller, J. A., The Chemkin Thermodynamic Database, Rep. SAND 87—8215, Sandia National Laboratories, Livermore, CA.

[18] Kilpinen, P., Glarborg, P., and Hupa, M., "Reburning Chemistry: A Kineti Industrial Engineering Chemistry Research, Vol. 31, 1992, pp.1477-1490.

[19] Glarborg, P., Alzueta, M. U., Dam-Johansen, K., and Miller, J. A., "Kinetic Modeling of Hydrocarbon/Nitric Oxide Interactions in a Flow Reactor", Combustion and Flame, Vol. 115, 1998, pp. 1-27.

[20] Prada, L., and Miller, J. A., "Reburning using Several Hydrocarbon Fuels: A Kinetic Modeling Combustion Science and Technology, Vol. 132, pp. 225-250.

[21] Miller, J. A., and Bowman, C. T., "Mechanism and Modeling of Nitrogen Chemistry in Combustion", Progress Energy Combustion Science, Vol. 15, 1989, pp. 287-338.

[22] Kicherer, A., Splicthoff, H., Maier, H., and Hein, K. R. G., " The effect of different reburning fuels on NO_x-reduction," Fuel, Vol. 73, No. 9, 1994, pp. 1443-1446.

[23] Kilpinen, P., Glarborg, P., and Hupa, M., "Reburning Chemistry: A Kinetic Modeling Study", Industrial Engineering Chemistry Research, Vol. 31, 1992, pp.1477-1490.

[24] Chen, S. L. , McCarthy, J. M., Clark, W. D., Heap, M. P., Seeker, W. R., and Pershing, D.W., "Bench and Pilot Scale Process Evaluation of Reburning for In-Furance NO_x Reduction", Proceedings of Symposium on Combustion, 1986, Vol. 21, pp. 1159

[25] Mereb, J.B., and Wendt J. O. L., "Reburning mechanisms in a pulverized coal combustion", Proceedings of Symposium on Combustion, 1990, Vol 23, pp. 1273

[26] Burch, T. E., Tillman, F. R., Chen, W-Y, and Lester, T. W., Conway, R. B., and Sterling, A. M., "Partitioning of Nitrogenous Species in the Fuel-Rich Stage of Reburning", Energy and Fuels, Vol. 5, No. 2, 1991, pp.231-237.

[27] Smart, J. P., and Morgan, D. J., "The effectiveness of multi-fuel reburning in an internally fuel-staged burner for NO_x reduction", Fuel, Vol. 73, No. 9, 1994, pp. 1437-1442.

[28] Chen, W-Y, and Ma, L., "Effect of Heterogeneous Mechanisms During Reburning of Nitrogen Oxide", AIChE Journal, Vol. 42, No. 7, 1996, pp. 1968-1976.

DIRECT OBSERVATION OF THE CATALYTIC PRODUCTION OF DIMETHYL CARBONATE USING ON-LINE GC/MS

Brian C. Dunn, Jorg Pahnke, Dan Hopkinson, Edward M. Eyring, Department of Chemistry, University of Utah, Salt Lake City, UT 84112.

Genshan Deng, Jacek Dworzanski, Henk L.C. Meuzelaar, Ronald J. Pugmire, Department of Chemical and Fuel Engineering, University of Utah, Salt Lake City, UT 84112.

KEYWORDS: Dimethyl carbonate, fuel oxygenate, on-line GC/MS

INTRODUCTION

Dimethyl carbonate (DMC) has the potential to replace methyl *t*-butyl ether[1,2] (MTBE) as an oxygenate fuel additive for both diesel and gasoline engines.[3] Previous research has shown that the addition of DMC to gasoline or diesel fuel reduces all forms of emissions: hydrocarbons,[3] carbon monoxide,[4] oxides of nitrogen,[4-6] and particulate matter.[7,8] Numerous routes exist for the production of DMC: reaction of methanol with urea with an organotin catalyst,[9] activation of CO_2,[10-12] and the reaction between methyl nitrite and carbon monoxide.[13] A promising route to the industrial production of DMC is the oxidative carbonylation of methanol.[14,15] A drawback of DMC is the lack of knowledge regarding the reaction mechanism that could lead to the efficient industrial production in sufficient quantity to satisfy the enormous demand in the American fuel market. Discovering the reaction mechanism should allow more efficient catalysts for the production of DMC to be developed and could facilitate the widespread adoption of DMC as an oxygen-containing fuel additive. We are investigating the reaction between methanol, carbon monoxide, and oxygen that produces DMC as one product:

$$2CH_3OH + CO + \frac{1}{2}O_2 \xrightarrow{Cu^{2+}} O = C(OCH_3)_2 + H_2O \qquad (1)$$

In order to obtain detailed information about the underlying reaction mechanisms and kinetics we are using a novel, on-line GC/MS technique developed at the University of Utah Center for Microanalysis and Reaction Chemistry (UUCMARC) that is capable of repetitively recording GC/MS profiles at 1 minute intervals, or less. This method can be used with a variety of chemical reactors and a broad range of reaction conditions[16-18] and enables definitive identification of many volatile or semi-volatile compounds in relatively complex reaction mixtures, while simultaneously producing kinetic profiles of all compounds as a function of time and temperature.

EXPERIMENTAL

The catalysts are prepared by dissolving the appropriate copper and/or palladium salt in methanol, adding the activated carbon support, and refluxing the mixture with vigorous stirring for four hours. The solvent is removed by vacuum distillation and the catalyst is dried under an inert atmosphere until completely free from solvent.

The reaction is studied by placing a mixture of the reactants and a sample of the previously prepared catalyst into a glass-lined stainless steel autoclave. The reaction chamber is suspended in a preheated fluidized sand bath in which the reaction can be carried out under either isothermal or temperature programmed conditions. The autoclave is interfaced to a GC/MS system that allows on-line identification and monitoring of all of the reaction produets in real time and the kinetic profile of the reaction is recorded.

A pressure reduction transfer line and a AVS-GC/MS system, where AVS denotes ambient vapor sampling, have been employed for real-time monitoring of the C1 reaction process by on-line analysis of volatile products from a high pressure batch reactor. The pressure reduction line is a 2 m long, 50 μm i.d. fused silica capillary with a volume flow of 0.8 ml/min as a function of the reaction pressure (the initial pressure: 150 psig, the highest pressure: 350 psig at 170 °C). The vapor sampling and GC functions of the system are contained in the Enviroprobe (FemtoScan Corp.), which attaches to a Hewlett-Packard model 5972 MSD (mass selective detector) via a modified, more power efficient version of the standard GC to MSD transfer line interface. The Enviroprobe utilizes an AVS inlet,[19] which performs the repetitive injection of vapor samples into the 10 m long, 250 μm i.d. fused silica capillary column with the temperature of 80 °C. The sampling time is one second and the sampling interval is two and a half minutes.

RESULTS AND DISCUSION

The on-line GC/MS system was found to perform quite well for this particular reaction process and reactor set-up. Besides providing direct information about the concentrations of organic reactants and products it also proved possible to directly monitor reaction gas components such as oxygen. Since the high partial pressures of these components tend to cause saturation of the molecular ion peak, as well as of the main fragment ion peaks, minor isotope peaks (e.g. $O^{18}O^{16}$ at m/z 34) can be used to monitor the kinetic profiles of these major reaction atmosphere constituents. This proved to be very informative, e.g. by showing that some catalysts cause rapid oxidation of CO to CO_2 at low temperatures, thereby making CO unavailable for the key reaction step with methanol as can be seen from Figure 1.

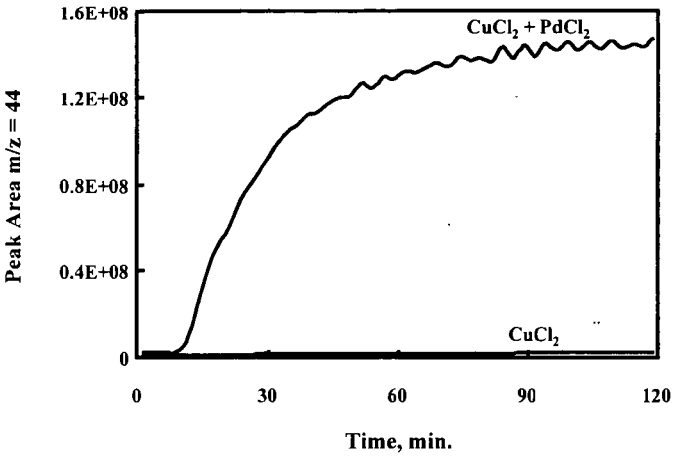

Figure 1. Comparison of CO_2 formation with two different catalysts: $CuCl_2$ + $PdCl_2$ and $CuCl_2$ only.

The effect of catalyst composition on the overall reaction was studied by preparing a series of catalysts using different metal salts. Six catalysts were prepared: $CuCl_2$, $Cu(Ac)_2$ (copper(II) acetate), $Cu(NO_3)_2$, $CuCl_2$ + $PdCl_2$, $Cu(Ac)_2$ + $Pd(Ac)_2$, and CuCl. The reactions were conducted under temperature-programmed conditions from 100 °C to 170 °C in order to observe the influence of temperature on the reaction chemistry. In all cases, varying proportions of dimethyl carbonate (DMC), dimethoxy methane (DMM), and methyl formate (MeFOR) were produced. When the acetate salts were employed, a fourth product, methyl acetate (MeAc), was also observed as seen from Figure 2. The product distributions present at the end of each experimental trial are given in Figure 3.

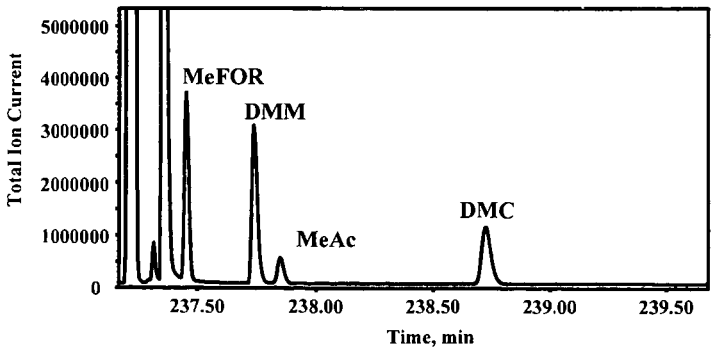

Figure 2. Chromatogram of the products from the following reaction: 0.5 g $CuAc_2$ catalyst, 5.0 g MeOH, 50 psi CO, 100 psi air, 170 °C .

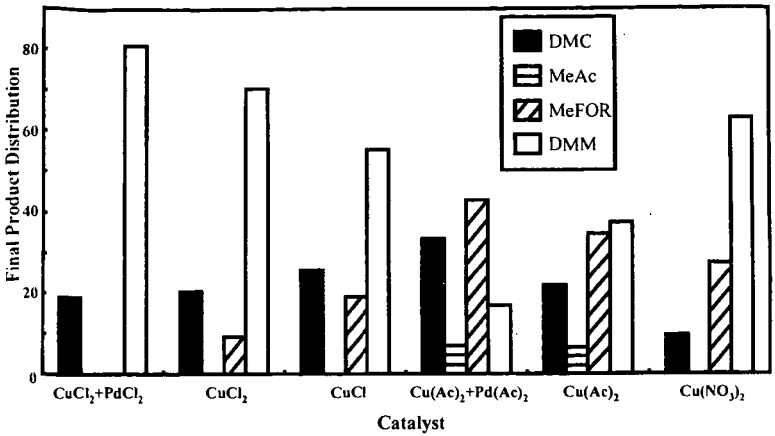

Figure 3. Final product distributions from six different catalysts. All reactions performed under the following conditions: 0.5 g catalyst, 5.0 g MeOH, 50 psi CO, 100 psi air, temperature programmed from 100 °C to 170 °C in 30 min. / 10 °C steps.

Palladium catalyzes the reaction of CO and O_2 to produce a large amount of CO_2, thereby reducing the amount of CO available for the production of DMC. The catalysts with acetate show significant activity, but because of the formation of a fourth product, methyl acetate, we chose the catalysts based on chloride salts for further study. The $Cu(NO_3)_2$ catalyst has the worst selectivity for DMC.

The reactant gas ratio influence was investigated with the CuCl catalyst by using differing amount of CO and air, but maintaining the same total pressure to minimize any pressure effects. Three different gas ratios were used and the product distributions are shown in Figure 4.

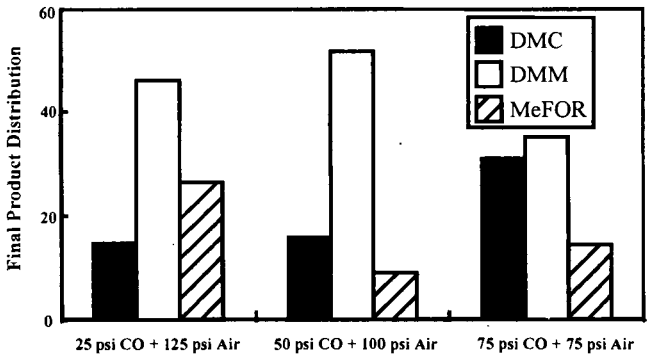

Figure 4. Final product distributions using CuCl catalyst with varying reactant gas ratios.

The influence of the support particle size was examined by using both the $CuCl_2$ and CuCl catalysts on three different activated carbon support sizes. The final peak areas were normalized by dividing the peak area of each reaction product by the peak area of the internal standard, n-hexane. The Tables 1 and 2 show the results.

Table 1. Final Peak Area Ratios using $CuCl_2$ Catalysts

Mesh	DMC Area Ratio	DMM Area Ratio	MeFOR Area Ratio
4-14	0.7255	0.3647	0.9506
20-40	0.5784	1.715	0.3207
100	0.6982	0.4843	1.002

Table 2. Final Peak Area Ratios using CuCl Catalysts

Mesh	DMC Area Ratio	DMM Area Ratio	MeFOR Area Ratio
4-14	1.025	0.3724	1.008
20-40	0.8210	1.328	0.7746
100	0.7483	0.3387	0.7420
20-40 crush	0.8629	1.278	0.8092

Because no clear trend was evident from the first six experiments, the final experiment was conducted using the 20-40 mesh CuCl catalyst that had been crushed into a fine powder. The results indicate that using the 20-40 mesh catalyst, in both forms, leads to the production of a much larger amount of DMM than either the larger or the smaller support. This evidence led us to conclude that the 20-40 mesh catalysts were causing the reaction of DMC to form DMM. This hypothesis was tested by loading the reactor with a 10 wt. % solution of pure DMC in methanol, $CuCl_2$ catalyst on 20-40 mesh support, and oxygen (from air). Figure 5 represents the results from that experiment.

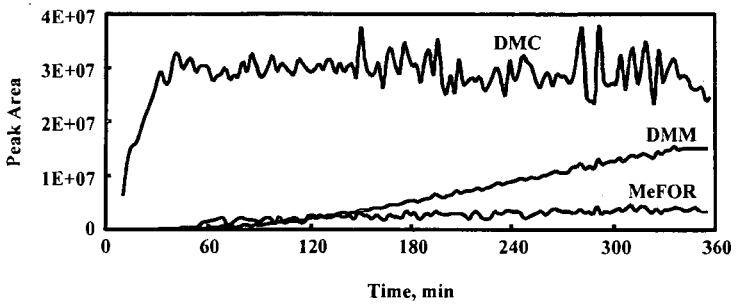

Figure 5. 10 wt. % DMC in methanol and CuCl catalyst.

DMM did gradually appear, but the signal from DMC did not decrease as predicted. The source of the DMM was not the oxidation of DMC, but an independent process. This was tested by charging the autoclave with $CuCl_2$ catalyst on 20-40 mesh, methanol, and oxygen (from air). No CO was added to inhibit the formation of DMC. Figure 6 is the result from that experiment.

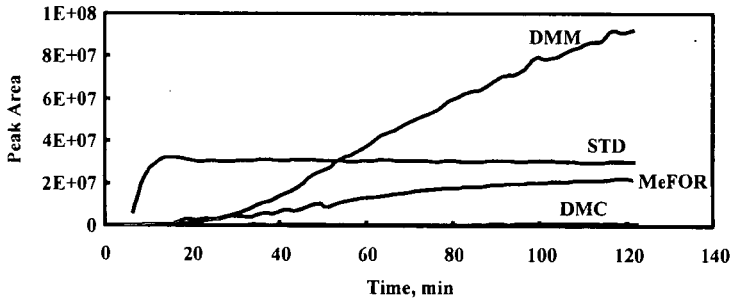

Figure 6. Methanol, $CuCl_2$ catalyst, and air reacting to form DMM.

Only DMM and MeFOR, the two unwanted products, were formed and at nearly the same rate as in a previous experiment in which CO was added.

CONCLUSIONS

The reaction that forms DMM and MeFOR is independent of the reaction that forms DMC. It should be possible to find a different catalyst that is much more selective for DMC due to these uncoupled reactions. From the Tables, it is clear that $CuCl_2$ and CuCl give rise to very similar product distributions. This leads us to conclude that the Cu^+ ion is most likely being oxidized to Cu^{2+} by the O_2 present inside the reactor. Neither the Cu^+ nor the Cu^{2+} catalyst offers a significant advantage over the other. The relationship between support particle size and reactivity appears to be more complicated than originally expected. This phenomenon is currently under investigation.

ACKNOWLEDGMENTS

Financial support by the U.S. Department of Energy, Fossil Energy Division, through the Consortium for Fossil Fuel Liquefaction Sciences, Contract No. UKRF-462633-99-200, is gratefully acknowledged.

REFERENCES

1. Kirchstetter, T. W.; Singer, B. C.; Harley, R. A.; Kendall, G. R.; Traverse, M. *Environ. Sci. Technol.*, **1999**, *33*, 318-328.

2. Gouli, S.; Lois, E.; Stournas, S. *Energy & Fuels*, **1998**, *12*, 918-924.

3. Pacheco, M. A.; Marshall, C. L. *Energy & Fuels*, **1997**, *11*, 2-29.

4. Japanese Patent 61[1986]-207496; Imoura, S.; Matsushita, D. "Fuel for Internal Combustion Engine": assigned to Toyo Soda Industry; **1986**.

5. Stoner, M.; Litzinger, T. "Effects of Structure and Boiling Point of Oxygenated Blending Compounds in Reducing Diesel Emissions"; SAE Technical Paper Series; **1999**; 1999-01-1475.

6. Murayama, T.; Zheng, M.; Takemi, C.; Oh, Y.; Fujiwara, Y.; Tosaka, S.; Yamashita, M.; Yoshitake, H. "Simultaneous Reductions of Smoke and Nox from a DI Diesel Engine with EGR and Dimethyl Carbonate"; SAE Technical Paper Series; **1995**; 952518.

7. US Patent 4,891,049; Dillon, D. M.; Iwamoto, R. Y. "Hydrocarbon Fuel Composition Containing Carbonate Additive"; assigned to Unocal; **1990**.

8. US Patent 4,904,279; Kanne, D. M.; Iwamoto, R. Y. "Hydrocarbon Fuel Composition Containing Carbonate and Dicarbonate Additives"; assigned to Union Oil; **1990**.

9. US Patent 5,902,894; Ryu, J. Y. "Process for Making Dialkyl Carbonates"; assigned to Catalytic Distillation Technologies; **1999**.

10. Sakakura, T.; Saito, Y.; Okano, M.; Choi, J.; Sako, T. *J. Org. Chem.*, **1998**, *63*, 7095-7096.

11. Cheong, M.; Kim, S.; Park, J. *New J. Chem.*, **1997**, *21*, 1143-1145.

12. Tomishige, K.; Sakaihori, T.; Ikeda, Y.; Fujimoto, K. *Cat. Lett.*, **1999**, *58*, 225-229.

13. Matsuzaki, T.; Ohdan, K.; Asano, M.; Tanaka, S.; Nishihira, K.; Chiba, Y. *J. Chem. Soc. Japan*, **1999**, 15-24.

14. Yanji, W.; Xinqiang, Z.; Baoguo, Y.; Bingchang, Z.; Jinsheng, C. *Applied Catalysis, A: General*, **1998**, *171*, 255-260.

15. Tomishige, K.; Sakaihori, T.; Sakai, S.; Fujimoto, K. *Applied Catalysis, A: General*, **1999**, *181*, 95-102.

16. Meuzelaar, H.L.C. "Comparison of On-line MS Techniques for Complex Reactive Systems," *Proceedings of the Specialists Workshop on Applications of Free-Jet Molecular Beam, Mass Spectrometric Sampling*, October 12-14, Estes Park Center, CO, NTIS, **1994**, NREL-CP-433-7748, 57-64.

17. Meuzelaar, H.L.C.; Liu, K.; Jakab, E. "Development of On-Line Chemical Speciation and Microsimulation Techniques for High Pressure Conversion Reactions in Coals & Waste Materials," *Proceedings of the 1994 U.S. Dept. of Energy Coal Liquefaction and Gas Conversion Contractors' Review Conference*, September 7-8, Pittsburgh, PA, **1994**, 637-649.

18. Nie, X.; McClennen, W.H.; Liu, K.; Meuzelaar, H.L.C. "Development of On-Line GC/MS Monitoring Techniques for High Pressure Fuel Conversion Processes," *ACS Preprints, Division of Fuel Chemistry*, **1993**, 38 (4), 1147-1155.

19. Arnold, N.S.; McClennen, W.H.; Meuzelaar, H.L.C. "Vapor Sampling Device for Rapid Direct Short Column Gas Chromatography/Mass Spectrometry Analyses of Atmospheric Vapors," *Analytical Chemistry*, **1991**, 63, 299-304.

ISOTOPIC TRACING OF PARTICULATE MATTER FROM A COMPRESSION-IGNITION ENGINE FUELED WITH ETHANOL-IN-DIESEL BLENDS

A. S. (Ed) Cheng[1], Robert W. Dibble[1], Bruce A. Buchholz[2]
[1]Department of Mechanical Engineering, University of California, Berkeley, CA
[2]Center for Accelerator Mass Spectrometry, LLNL, Livermore, CA

KEYWORDS: diesel particulate matter, oxygenate, isotope tracing, AMS

INTRODUCTION

Environmental and human health concerns over emissions from internal combustion engines continue to bring about increasingly stringent emissions standards and drive research into the use of non-conventional, cleaner-burning fuels. For compression-ignition (diesel) engines, oxygenated fuels have been shown to dramatically reduce particulate matter (PM) while also improving or maintaining acceptable levels of other regulated emissions (NO_x, HC and CO) [1-8]. The mechanisms through which oxygenates reduce PM, however, are not fully understood. In addition to changes in combustion chemistry, the influence of thermophysical properties on fuel injection and fuel-air mixing can play a significant role.

To gain further insight into the effect of oxygenates on diesel engine PM emissions, Accelerator Mass Spectrometry (AMS) was used to investigate the relative contribution to soot (the carbonaceous component of PM) from the ethanol and diesel fractions of blended fuels. AMS counts electrostatically accelerated nuclei (32.5 MeV for $^{14}C^{4+}$) in a simple particle detector [9]. Molecular isobars are completely disassociated in the charge changing process and any atomic isobars are discriminated in the detector. AMS is particularly efficient in detecting long-lived isotopes (10 y < $t_{1/2}$ < 100 My). The rarity of long-lived radioisotopes yields a much lower background than that achievable with stable isotopes. For example, the naturally occurring carbon isotopic abundances are: ^{12}C (98.9%), ^{13}C (1.1%), and ^{14}C ($1.2x10^{-10}$%). The natural background of ^{14}C is 10 orders of magnitude lower than the rare stable isotope ^{13}C and AMS achieves limits of quantitation for ^{14}C below 1×10^{-18} mol in individual samples (LOQ < 1 amol ^{14}C / mg C). The decrease in background yields much greater sensitivity for ^{14}C AMS over ^{13}C MS. Decay counting long lived isotopes is not efficient; counting 0.1% of the decays of a ^{14}C sample takes 8.3 years.

MATERIALS AND METHODS

In this study, contemporary grain ethanol (109 amol ^{14}C/mg C) served as an isotopic tracer in old carbon diesel fuel (0.26 amol ^{14}C/mg C). The ethanol was manufactured by Midwest Grain Products, Pekin, IL. The diesel was a CARB-certified No. 2 diesel fuel obtained from Golden Gate Petroleum, Hayward, CA. Properties of ethanol and the diesel test fuel are shown in Table 1. Because ethanol is soluble in diesel fuel in only small quantities, either an emulsifier (Span 85, also known as sorbitan trioleate) or a cosolvent (n-butanol) was used to prepare the ethanol-in-diesel blends. An ignition improver, di-tert-butyl peroxide (DTBP), was also used to compensate for the low cetane number of ethanol. The Span 85 and n-butanol were obtained from Spectrum Quality Products, Inc.; the DTBP was obtained from Pfaltz & Bauer. All fuel blend components were converted to AMS samples [10] and ^{14}C content was measured. The four different ethanol-in-diesel blends investigated are shown in Table 2. A high-speed, high-shear mixer (Greerco Model 1-LV Homomixer) was used to prepare the emulsified blends.

The experimental test engine is a 1993 Cummins B5.9 rated at 175 hp (131 kW). Engine specifications are listed in Table 3. The engine employs a mechanically-governed in-line fuel injection pump capable of injection pressures up to 115 MPa. No modifications were made to the test engine to optimize for operation on the test fuels.

Table 1. Ethanol and diesel fuel properties.

Fuel	Ethanol[a]	Diesel[b]
Density (kg/L)	0.7923	0.8473
Cetane number	<5	49.1
Sulfur (ppm)	-	98
SFC total aromatics (wt. %)	-	16.32
SFC PNA's (wt. %)	-	4.09
Nitrogen	-	< 5 ppm
Boiling point (°C)	78	-
Distillation by D86 (°C)		
IBP	-	173
10%	-	237
50%	-	299
90%	-	336
95%	-	347
EP	-	358
Lower heating value (MJ/L)	21.2	35.4

[a] from literature sources

[b] as determined by fuel analysis

Table 2. Test fuel blends (components listed in percent by volume).

Fuel Blend	Diesel	Ethanol	SPAN 85	n-butanol	DTBP
A	72.0	23.0	4.0	-	1.0
B	70.0	25.0	-	4.0	1.0
C	83.5	11.5	4.0	-	1.0
D	82.5	12.5	-	4.0	1.0

Table 3. Cummins B5.9 engine specifications.

Model year	1993
Displacement	5.88 liters (359 in^3)
Configuration	6-cylinder inline
Bore	102 mm (4.02 in)
Stroke	120 mm (4.72 in)
Compression ratio	17.6:1
Horsepower rating	175 hp @ 2500 rpm
Torque rating	420 ft-lb @ 1600 rpm
Aspiration	turbocharged and aftercooled
Injection timing (fixed)	11.5° BTDC

Prior to beginning any experiments, lab facilities were checked for fixed and aerosol ^{14}C contamination with AMS analyzed swipes and fullerene aerosol monitors. During the experiments, a steady-state engine speed-load condition of 1600 rpm and 210 ft-lbs (285 N-m) was used and measurements were made for PM, NO_x, HC and CO emissions, as well as for fuel consumption. Gaseous emissions (NO_x, HC and CO) were monitored using Horiba Instruments emissions analyzers and fuel consumption was measured via a load cell mounted under the fuel tank. PM was determined using a mini-dilution tunnel and gravimetric filter paper measurements. The filters (Pallflex Tissuquarz 2500QAT-UP) were conditioned overnight in petri dishes and weighed before and after PM loading on a Mettler UM3 microbalance. Filters were then sealed in plastic bags prior to preparation as AMS samples. Because of the limited quantity of contemporary grain ethanol obtained and time needed to collect sufficient PM mass for AMS analysis (~ 30 min. of engine operation), only one sample was collected for each test fuel.

In preparation for AMS analysis, the filters with collected PM were baked at 900 °C for 2 h prior to use to remove carbon residue and stored in sealed plastic bags after cooling. Filters were cut into 2 or 3 pieces and converted to graphite for AMS measurement of isotope ratios [10]. Isotope ratios were measured to within 1-8%. Relative uncertainties were governed primarily by counting statistics. The samples with very low ^{14}C content had larger uncertainties. AMS measures the isotope concentration of unknown samples relative to those of known standards. In these experiments we normalized to four identically prepared standards of Australian National University Sucrose [11].

RESULTS AND DISCUSSION

Brake-specific emissions and fuel consumption results from the baseline diesel fuel and the four test fuel blends are shown in Table 4. A graphical representation of PM and NO_x emissions is shown in Figure 1. As anticipated, the general trend was towards lower PM emissions with higher levels of oxygenate (note that the cosolvent n-butanol is itself also an oxygenate), although an anomaly exists in that fuel blend C produced a 10% increase in PM. The data also indicates that the homogeneous cosolvent blends are more effective at reducing PM emissions compared to the emulsified blends. NO_x emissions from the ethanol-in-diesel blends were 22% to 27% lower than that of the baseline diesel and did not show large variation across the different blends. Emissions of both HC and CO increased, but remained very low as is typical with diesel engine combustion. Fuel consumption was higher with the test fuel blends due to the lower energy density of ethanol.

Table 4. Brake-specific emissions and fuel consumption results (g/kW-hr).

FUEL	Diesel	Blend A	Blend B	Blend C	Blend D
PM	0.032	0.025	0.012	0.035	0.029
NOx	6.28	4.58	4.90	4.92	4.88
HC	0.084	0.160	0.172	0.203	0.224
CO	0.312	0.517	0.625	0.358	0.371
bsfc	230	249	270	261	256

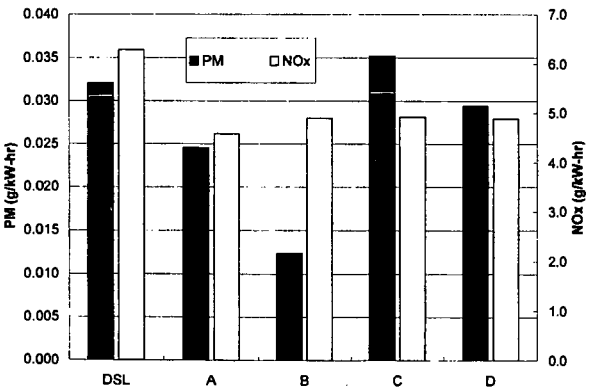

Figure 1. Brake-specific emissions of PM and NO_x.

Isotope ratios of the fuel components are reported in Table 5. The ^{14}C content of the petroleum derived components are low as expected. The emulsifier, Span 85, has a contemporary ^{14}C content, indicating it is derived from biological products.

Table 5. Carbon-14 content of fuel components.

COMPONENT	amol ^{14}C / mg C
Diesel	0.26
Ethanol	109
n-butanol	0.31
Span 85	109
DTBP	0.17

Measured isotope ratios (IR) contain contributions from all the components (and possibly more) shown in Eq. 1.

$$IR_{sample} = \frac{^{14}C_{diesel} + ^{14}C_{ethanol} + ^{14}C_{absorbed} + ^{14}C_{emulsifier} + ^{14}C_{cos olvent} + ^{14}C_{additives}}{C_{diesel} + C_{ethanol} + C_{absorbed} + C_{emulsifier} + C_{cos olvent} + C_{additives}} \quad (1)$$

In practice we try to reduce the number of terms of this equation by limiting the number of components or rendering some terms negligible through judicious choice of compounds or experimental conditions. Through the use of appropriate controls we determined the contributions of the various components in Eq. 1. Traditional tracer experiments depend on radioactive decay for detection and are usually dominated by a highly labeled tracer with very small mass. In our case, the labeled tracer was not radioactive in the traditional sense and contributed a significant amount of carbon in the measured isotope ratio. We sought to determine the mass of tracer ethanol in the soot and need to consider the products of carbon mass and the isotope ratios. The total carbon mass is expressed in Eq. 2.

$$M_{sample} = M_{diesel} + M_{ethanol} + M_{absorbed} + M_{emulsifier} + M_{cosolvent} + M_{additive} \quad (2)$$

The product of the isotope ratio and carbon mass of each sample is the sum of the product of each component as described in Eq. 3.

$$IR_{sample}M_{sample} = \sum_{i=component} IR_i M_i \quad (3)$$

Equations 2 and 3 can be solved to determine the mass contributions of each component with knowledge of the isotope ratios of the components and a series of controls adding each component to the fuel mixture.

The isotope ratios of the filter samples loaded with PM from the fuel blends and the associated controls were elevated due to the absorption of atmospheric CO_2 and other carbon compounds on the soot during equilibration. Atmospheric CO_2 has approximately the same ^{14}C content as ethanol, 109 amol ^{14}C / mg C. The quantity of absorbed carbon depends on the surface area of the soot and length of time spent equilibrating in the atmosphere. It should scale with the mass of soot deposited on the filters when equilibration times are constant. Separate control blanks were collected for soot samples from fuel blends A and B and from blends C and D. Assuming that all the sorbed carbon was contemporary, the mass of carbon absorbed with the separate sets of filters were 2.4% and 4.2% for blends A and B and blends C and D, respectively. These values for mass fraction of absorbed atmospheric carbon were propagated in the soot samples obtained form the fuel blends and the controls that included emulsifier or cosolvent without the ethanol.

Equations 2 and 3 were used to solve for the fractional mass of carbon in the soot from the emulsifier and ethanol. The mass fraction of carbon in the soot was not measured so all isotope measurements are expressed as fractions of soot carbon rather than absolute numbers. Since the ^{14}C content of the cosolvent and ignition improver were essentially the same as the diesel fuel,

their contributions to the carbon soot mass could not be determined in our limited experiment. Either n-butanol or DTBP could be traced if desired, but we were not interested in obtaining isotope labeled material for this purpose. Our interest was primarily in tracing the ethanol. The contributions of the ethanol to the carbon mass in the soot is displayed in Table 6. Since the emulsifier is only 4% by volume in blends A and C, its contribution to the carbon mass is not large.

As the data in Table 6 shows, ethanol contributed less to soot than did the diesel in the all of the test fuel blends. Results also indicate that the percent of fuel ethanol contributing to soot is higher for the emulsified blends A and C compared to the cosolvent blends B and D. Along with the brake-specific emissions data, this suggests that the chemical mechanisms that inhibit soot formation and/or promote soot oxidation are different depending on the nature in which ethanol is blended with the diesel fuel.

Table 6. Contributions of ethanol to carbon soot mass. Fuel blends A and C used the emulsifier Span 85 while Blends B and D used n-butanol as a cosolvent.

Fuel blend	Ethanol volume % (fuel)	Ethanol carbon mass % (fuel)	Ethanol carbon mass % (soot)
A	23.0	15	8.6
B	25.0	16	6.3
C	11.5	7	4.7
D	12.5	8	3.8

CONCLUSIONS

Gravimetric filter paper measurements and isotopic tracing of PM reveal that ethanol-in-diesel blends reduce PM emissions from compression-ignition engines in a manner which results in a lower ethanol contribution to soot relative to its fraction in the fuel blend. Experimental results also indicate that homogeneous blends of ethanol and diesel behave differently than emulsified blends and yield lower PM emissions.

This study also demonstrated the power of using AMS to perform isotope tracing without using any specially labeled material. No radioactive material was used in any part of these experiments. Therefore, no mixed wastes (radioactive and hazardous) were generated, greatly simplifying disposal [12]. In practice, one could label any fuel additive or component and follow its fate in particulate emissions or exhaust gases. The sub-attomole sensitivity of ^{14}C-AMS can be used to separate components of exhaust gases (e.g., hydrocarbons, CO, CO_2) and quantify fuel stock contributions. Particulate separators can also be used to look at the fate of fuel components in different sized soot emissions.

ACKNOWLEDGEMENTS

Support was provided by a LLNL Center for Accelerator Mass Spectrometry Mini-grant. Work completed at LLNL was supported under DOE contract W-7405-ENG-48.

REFERENCES

1. Cheng, A. S. and R. W. Dibble. "Emissions Performance of Oxygenate-in-Diesel Blends and Fischer-Tropsch Diesel in a Compression Ignition Engine," SAE paper 1999-01-3606, 1999.
2. Wong, G. et al. "Low Soot Emission from a Diesel Engine Fueled with Dimethyl and Diethyl Ether," WSS/CI paper 95F-162, October 1995.

3. Liotta, F. J. and D. M. Montalvo. "The Effect of Oxygenated Fuels on Emissions from a Modern Heavy-Duty Diesel Engine," SAE paper 932734, 1993.
4. Fleisch, T. et al. "A New Clean Diesel Technology: Demonstration of ULEV Emissions on a Navistar Diesel Engine Fueled with Dimethyl Ether," SAE paper 950061, 1995.
5. McCormick, R. L., J. D. Ross and M. S. Graboski. "Effect of Several Oxygenates on Regulated Emissions from Heavy-Duty Diesel Engines," Environmental Science & Technology, vol. 31, no. 4, 1997.
6. Bertoli, C., N. Del Giacomo and C. Beatrice. "Diesel Combustion Improvements by the Use of Oxygenated Synthetic Fuels," SAE paper 972972, 1997.
7. Miyamoto, N. et al. "Smokeless, Low NO_x, High Thermal Efficiency, and Low Noise Diesel Combustion with Oxygenated Agents as Main Fuel," SAE paper 980506, 1998.
8. Maricq, M. M. et al. "The Effect of Dimethoxy Methane Additive on Diesel Vehicle Particulate Emissions," SAE paper 982572, 1998.
9. Vogel, J. S., Turtletaub, K. W., Finkel, R., and Nelson, D. E. *Anal. Chem.* 1995, *67*, A353-A359.
10. Vogel, J. S. *Radiocarbon* 1992, *34*, 344-350.
11. Polach, H. A., In *Proceedings of the 9th International Conference on Radiocarbon*; Berger, R., Suess, H., Eds.; UC Press: Berkeley/Los Angeles, CA, 1979; pp. 115-124.
12. 10 CFR 20.2005 *Fed. Reg.*, 1991, *56*, 434.

CHARACTERIZATION OF CHEMICAL COMPOSITION AND SIZE OF DIESEL EXHAUST PARTICULATE MATTER BY LDITOF/MS.

J. Suro*, Q. Chen, I.M. Kennedy, T.A. Cahill and P.B. Kelly

University of California, Davis, California 95616

Key Words: Time of flight mass spectrometry; Diesel soot; Polycyclic aromatic hydrocarbons

Introduction

Diesel engines see extensive use due to their high efficiency and suitable torque characteristics. In general diesel engines have lower carbon monoxide and hydrocarbon emissions than spark-ignition engines. However, they are known to create much larger amounts of particulate matter and polycyclic aromatic hydrocarbons (PAHs) and their derivatives. Contributing factors are higher temperatures and pressures in the combustion process together with larger initial concentrations of aromatics in the diesel fuel.

The presence of the aromatic compounds in the air represents a potential hazard to human health. Several PAHs and nitro-PAHs have been identified as carcinogenic and potentially carcinogenic compounds (Ref. 1). The extent of human exposure to PAHs and their derivatives depends on the partitioning between the gas and particle phases as well as the size distribution of the particle fraction containing the PAHs. There is a much greater potential carcinogenic effect if the PAHs are components of particles that penetrate and deposit into the bronchia and alveoli of the lungs. Studies show that a major fraction of particles that are 1.0 μm or less in diameter might deposit in the air ways and lungs (Ref. 2). Moreover, some recent studies have correlated health effects with the concentration of atmospheric particles, yet have failed to identify the causative agents (Ref. 3). Since the toxicity of particles from different sources varies widely, such studies would be much more valuable if the particles from a source were characterized with respect to size and composition.

Traditional methods for the determination of PAHs and nitrated PAHs are based on gas chromatography/mass spectrometry or liquid chromatography with fluorescence techniques for detection. Both approaches are time consuming, may require solvent extraction and separation, are expensive, and in most cases require multiple runs (Ref. 4). In this study performed on diesel soot, we demonstrate the applicability of Laser Desorption Ionization Time of Flight Mass Spectrometry (LDITOF/MS) as a rapid screening method in the analysis of particulate matter collected and segregated by particle size using a multiple stage portable impactor. LDITOF/MS is capable to generate parent ion dominated spectra with low fragmentation from samples containing particles in a specific size range, which makes LDITOF/MS an excellent technique for the screening for PAHs in complex mixtures without need for solvent extraction and separation.

Experimental

The source of diesel exhaust particulate matter was an experimental direct injection 1 cylinder diesel engine aspirated at normal pressure (no turbocharger was used). Samples were collected with the engine idling warm at 2,000 rpm. Reformulated California grade diesel fuel (low sulfur content) was used for the experiment.

Diesel soot samples were collected using a three stage portable impactor developed by the Delta Group at UC Davis (Ref. 5). The impactor was equipped with aluminum foil strips attached to rotary drums that, during sampling, rotated at a fixed angular speed exposing the attached aluminum strip to an inlet nozzle. The dimensions of the inlet nozzle determined the range of size of particles that hit the surface of the strip. As the drum rotates the segment of aluminum strip exposed to the inlet changed continuously, resulting in a deposition of sample with a time reference. A cyclone pump operating with a flow rate of 22.7 l min^{-1} allowed for collection of particles less than 2.5 μm in aerodynamic diameter. The 50% cut point of such an impactor has been validated both in extensive field and laboratory studies (Ref. 5 and references there in).

Samples were obtained positioning the impactor at 20 cm from the exhaust of the diesel engine. A Nucleopore® filter at the external inlet prevented coarse matter from entering the impactor. This filter permits particles of diameters smaller than 2.5 μm to penetrate into the impactor.

Particles with aerodynamic diameter between 2.5 μm to 1.15 μm were collected on the first stage of the impactor (denoted stage A). The second stage collected particles within the size range 1.15 μm to 0.24 μm (denoted stage B). The third stage accumulated particles of size 0.24 μm to 0.07 μm (denoted stage C). Particles not trapped on the aluminum strips were collected on a 0.01 μm porous teflon filter at the impactor outlet.

The laser desorption ionization time of flight mass spectrometer used has been described in previous publications (Ref. 6). Ultraviolet radiation of 266 nm produced from the fourth harmonic of a Nd:YAG laser with a 2.5 ns pulse width was used to desorb and ionize the sample. The UV laser beam was focused into the source region through a 250 mm focal length S1-UV quartz lens. The beam was directed incident to the sample surface at 45°. Neutral density optical filters were used to reduce the laser power to 10^6 W/cm^2 at the focal point on the sample surface. The beam diameter at the focal point was about 90 μm. A time delay of 250 ns in the application of the extraction potential at the source allowed time for prompt decay of metastable ions and improved overall resolution.

Particulate matter from each stage and from the inlet and outflow filters of the impactor were analyzed using LDITOF/MS. Segments of the aluminum foil from the impactor were attached to the sample probe and loaded into the TOF/MS. Each spectrum recorded was the sum of 240 randomly located laser shots. Blank filters and aluminum foil were checked for contaminants. Both positive and negative mass spectra were collected and analyzed.

Results

Positive ion mass spectra for five diesel particle size ranges matter are shown in Figure 1. Spectrum in *1a)* was obtained from the particles trapped at the external inlet filter with diameters larger than 2.5 μm; *1b)* shows the spectrum resulting from particles with aerodynamic diameter between 2.5 μm to 1.15 μm, stage A; *1c)* from the size range 1.15 μm to 0.24 μm, stage B; *1d)* was obtained from particles in the stage C whose diameters range between 0.24 μm and 0.07 μm. At the bottom *1e)* display the ion yield obtained from the outlet filter, with particles smaller than 0.07 μm.
Low mass peaks (identified as PAHs), are more abundant in large particles, > 2.5 μm diameter, than small particles, < 0.07 μm diameter. The general trend of the shift of PAH mass, with high mass PAH being associated with the fine particulate is clear in Figures *1a)* through *1e)*. Only the smallest particles, 0.07 μm have significant amounts of PAH with mass greater than 400 amu. In contrast, in *1a)* ion yield of mass above 400 Da decreases rapidly.

Two series of PAH ions are observed in all the positive ion spectra in Figure 1. The two series are most apparent in Figure *1e)*. The first series is comprised of m/z: 178, 202, 228, 252, 276/278, 302, 326/328, 350/352, 374/376, 398/400/402, and higher masses.
The second series has twice the frequency as the first series, with every other peak overlapping (with some exceptions) with the first series. The second series is comprised of m/z 190, 202, 216, 226, 240, 252, 266, 276, 290, 302, 326, 326, 342, 350/352, 366, and higher masses. Both series have been labeled in Figure *1b)*. A surprisingly large potassium signal is observed in the smallest particles, Figure *1e)*.

Negative ion spectra of the diesel particulate matter are shown in Figure 2. As in the case of the spectra of positive ions, each plot corresponds to a different fraction. From *2a)* to *2e)*, spectra were taken from particles larger than 2.5 μm; from 2.5 μm to 1.15 μm, stage A; from 1.15 μm to 0.24 μm, stage B; ranging from 0.24 μm to 0.07 μm, stage C; and smaller than 0.07 μm.
In contrast to positive ion spectra, the highest mass negative ions (m/z: 369, 414, and 447) are associated with the larger particles.
Inorganic ions, OH^-, Cl^-, NO_2^- and NO_3^- are observed for all five particle size range.
Very fine particles, < 0.07 μm, show significantly higher HSO_4^- than any of the spectra for larger particles.

Discussion

In a recent study by Reilly and collaborators (Ref. 7), organic composition of individual particles of diesel soot are obtained using an excimer laser for ablation ionization. Using this technique they are able to detect known compounds in diesel soot and to establish some differences in

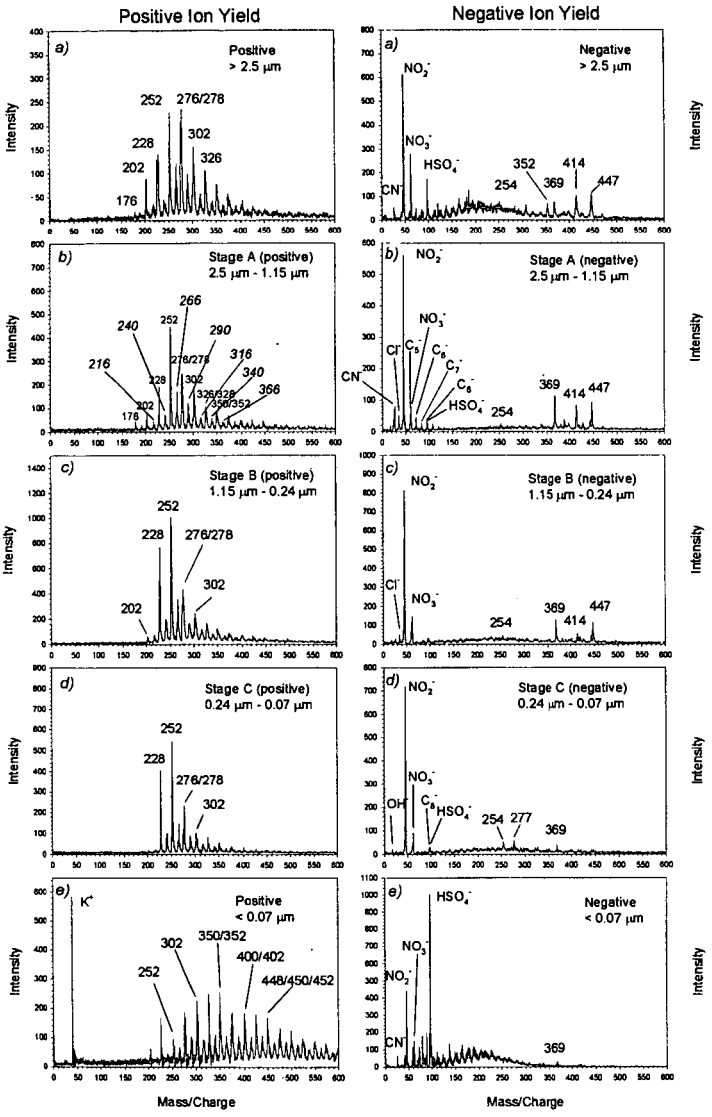

Figure 1. Positive ion mass spectra for five diesel particle size ranges.

Figure 2. Negative ion mass spectra for five diesel particle size ranges.

chemical composition according to particle size. However their method involves unavoidable fragmentation that obscures their results. On other study, Hankin and John (Ref. 8) examine the chemical composition of individual particles of diesel soot SRM 1650. In their experiment using LDITOF/MS, individual particles fixed to a sample support are subject to microlaser beam that desorbs compounds from the particle, and a second beam ionizes the compounds in the plume of desorbed material. The Hankin and John TOF/MS analysis of SRM 1650 yielded the mass of some certified compounds in their sample as well as some other compounds not certified but

known to be present in such standard such as alkylated PAHs. The Hankin and John study examined only very large particles (~ 20 μm).

In our study we report the first mass spectra of particles that were sized using an impactor. Working with a laser spot of 90 μm of diameter, the signal was derived from many particles at the same time thus obtaining reproducible results that are representative of a particular particle size range. In positive ion mode, the most intensive peaks in Figure 1 correspond to PAHs commonly found in diesel exhaust. The spectrum from stage A shows peaks corresponding to the mass of PAHs listed in Table I. Moreover from Figure 1, it is clear that many other PAHs are present in the samples. The first series corresponds to PAHs isomers containing only 6 member rings. The second series, with every other peak overlapping with the first series (with a few exceptions), corresponds to PAHs containing five member rings.

Table I
PAHs commonly found in diesel soot.

PAH	mass
phenathrene	178
fluoranthene	202
pyrene	202
benz[a]anthracene	228
chrysene	228
benzo[a]pyrene	252
benzo[e]pyrene	252
benzo[k]fluoranthene	252
perylene	252
benzo[ghi]perylene	276
indeno[123-cd]pyrene	276

Spectra in Figure 1 shows identifiable peaks up to mass 448; some authors have detected such mass in environmental samples and have assigned tentatively benz[a]ovalene as the most probable identity of the isomer (Ref. 9). Table II list a few possible assignments to peaks in the second series (Ref. 10).

Soot particles emitted from a diesel engine are usually observed as chain aggregates composed of several tens to hundreds of primary spherical particles. Ishiguro and collaborators (Ref. 11), have found that the structure of such spherical particles consist on an inner core surrounded by an outer shell. The inner core of 0.010 μm are composed of nonplanar molecules. The surrounding outer shell is compose of micro crystallites comprising several polycyclic aromatic hydrocarbon layers oriented concentrically in a soot particle. During shell formation, molecules, radicals, or ions including two to four carbon atoms could contribute the surface reactions promoting the polycyclic growth of the graphitic crystallites. Those observations by Ishiguro and collaborators support the assignment of peaks in Figure 1 as PAHs compounds. The extreme high mass range of PAHs observed for small particles would not be observable by traditional GC/MS.

Table II. Few possible mass assignments for peaks in the second series (see text).

Formula	Mass (Da)	Compounds
$C_{16}H_{10}$	202	Fluoranthene
$C_{17}H_{12}$	216	Cyclopentaphenanthrene
		Cyclopentaanthracene
		Benzofluorene
$C_{18}H_{10}$	226	Benzo(ghi)fluoranthene
$C_{19}H_{12}$	240	Cyclopentapyrene
		Benzofluoranthene
		Cyclopentachrysene
		Benzopyrene
$C_{20}H_{12}$	252	Benzocyclopentanthracene
$C_{21}H_{14}$	266	Benzocyclopentanthracene
		Indenophenanthrene
		Dibenzofluorene
		Benzochrysene
$C_{22}H_{12}$	276	Benzocyclopentapyrene
$C_{23}H_{14}$	290	Benzocyclopentachrysene
		Dibenzopyrene
$C_{24}H_{14}$	302	Cyclopentindenophenanthrene
$C_{25}H_{16}$	316	Benzindenophenanthrene
$C_{26}H_{14}$	326	Indenoperylene
$C_{27}H_{16}$	340	Tribenzopyrene
$C_{28}H_{14}$	350	Diindenopyrene
$C_{29}H_{18}$	366	Dibenzopentacene

Diesel soot particles exhibit size ranging (Ref. 12) from 4 μm to 0.04 μm, with a peaking distribution about 0.1 μm. Our study reveal that there are differences in the chemical contents of particles in such range. This information may be relevant in toxicological studies that assess the health hazard imposed by the continuous use of diesel engines. Toxicological assessments, regulation and development of cleaner running diesel engines(Ref. 13) require development of analytical methods that can examine the exhaust by particle size. Our results may provide a guide for pollutants reduction in the emissions of diesel engines based in a better understanding of the process that generate soot and pollutants.

Conclusions

The ability to use TOFMS to characterize the chemical composition of diesel soot particles captured using an impactor has been demonstrated. The analysis of size segregated particles from the impactor was performed without further preparation loading directly a sample collected on aluminum foil into the MS chamber. Results indicate a variation of the compound contents according to particle size. In general finer particles have high concentration of extremely large PAHs, potassium, and sulfate. The larger particles contain lower mass PAHs.
Our data show the presence of many PAHs in diesel soot that have not been fully characterize as compounds found in diesel soot. Our method detected extremely large PAHs not amenable to GC/MS analysis.

Our technique may be useful for the characterization of emissions of different sources according to the size of the particles. Accurate assessment of human health hazards associated with particulate matter requires chemical analysis associated with particle size and source. This information would be very valuable for addressing the question of which are the most important factors on the bioactivity associate with different class of particles.

References

1. R. Bhatia, P. Lopipero and A.H. Smith, Diesel exhaust exposure and lung cancer, Epidemiology 1998, **9**, 84.

2. US Environmental Protection Agency, 1996. Air quality Criteria for Particulate Matter, vol. I, EPA/600/P-95/001aP, Washington, DC.

3. Dockery, D.W.; Schwartz, J.; Spengler, J.D. Air pollution and daily mortality – associations with particulates and acid aerosols. Environ. Res. 1992, **59**, 362.

4. Scheepers, P.T.J., Velders, D.D., Martens, M.H.J., Noordhoek, J., Bos, R.P. Gas chromatographic-mass spectrometric determination of nitro polycyclic aromatic hydrocarbons in airborne particulate matter from workplace contaminated with diesel exhaust. J. Chromatogr. A 1994, **A 677**, 107.

5. Malm, W.C., Sisler, J.F., Huffman, D., Eldred, R.A. and Cahill, T.A. Spatial and seasonal trends in particle concentration and optical extinction in the United States. J. Geophys. Res., 1994, **99**, Sec. D, 1347.

6. Bezabeh, D.Z., Allen, T.M., McCauley, E.M. and Kelly, P.B. Laser desoption ionization time of flight mass spectrometry of nitrated polycyclic aromatic hydrocarbons. J. Am. Soc. Mass Spect., 1997, **8**, 630.

7. Reilly, P.T.A., Gieray, R.A., Whitten, W.B., and Ramsey, J.M. Real time characterization of the organic composition and size of individual diesel engine smoke particles. Environ. Sci Technol. 1998, **32**, 2672.

8. Hankin, S.M. and Jonh P. Laser time of flight mass analysis of PAHs on single diesel particles. Anal. Chem. 1999, **71**, 1100.

9. Dale, M.J.; Downs, O.H.J.; Costello, K.F.; Wright, S.J.; Langridge-Smith, P.R.R.; Cape, J.N. Environ. Pollut. 1995, **89**, 123.

10. Sander, L.C. and Wise, S.A. Polycyclic Aromatic Hydrocarbon Structure Index. NIST Special publication 922. 1997.

11. Ishiguro, T.; Takatori, Y. and Akihama K. Microstructure of diesel soot particles probed by electron microscopy: first observation of inner core and outer shell. Combustion and Flame, 1997, **108**, 231.

12. Kerminen, V.M. et. al. Characterization of the particle phase in the exhaust from diesel car. Environ. Sci. Technol. 1997, **31**, 1883.

13. Rakopoulos, C.D.; Hountalas, D.T.; Taklis, G.N. and Tzanos, E.I. Analysis of combustion and pollutants formation in a direct injection diesel engine using a multi-zone model. International Journal of Energy Reasearch, 1995, **19**, 63.

CO-COKING OF COAL AND PETROLEUM RESID MIXTURES FOR PRODUCTION OF COAL-BASED JET FUEL

Anne E. Fickinger, Mark W. Badger, Gareth D. Mitchell and Harold H. Schobert
The Energy Institute
Coal Utilization Laboratory
The Pennsylvania State University, University Park, PA. 16802

Keywords: Coal/resid co-coking, coal-derived jet fuels, coke formation, delayed coking.

Introduction

The next generation of high Mach aircraft will utilize jet fuel to serve two main purposes. First the fuel will be used as a propellant. The second function of the fuel will be to serve as a heat sink for the aircraft's subsystem. As a result the fuel will be exposed to thermally stressing temperatures that exceed 450 °C, where pyrolytic degradation can occur. If solid deposits form in the fuel as a result of this degradation, plugging of the fuel lines can result. The presently used petroleum-derived jet fuel, JP-8, lacks the necessary hydroaromatic compounds that increase the thermally stability of the fuel. Fuel containing coal-derived components, however, would contain 2-3 ring hydroaromatics that increase the thermal stability of the fuel. However, past methods for obtaining coal-derived liquids are not economical.

There are two main processes for production of coal-derived liquids, coal liquefaction and coal pyrolysis [1,2]. Coal liquefaction produces desired low-boiling aromatic hydrocarbons, which are then upgraded. However the process involves high hydrogen pressures, which pose economic concerns [1]. At the other end of the spectrum, coal pyrolysis is a process that yields coal-derived liquids using mild operating conditions. However, the main products obtained from coal pyrolysis are water, carbon oxides and light hydrocarbon gases while the desired coal-derived liquids are produced in low quantity [2].

In our search for an alternative pathway for producing coal-derived liquids, the desire to incorporate a well-established industrial process became our driving force. Since oil refineries utilize delayed cokers to convert low-valued feedstocks into useful products such as low boiling distillates, it was decided to examine such a process to see if it could be modified to produce coal-derived liquids.

Delayed coking is a commercially used process to obtain quality coke and light hydrocarbon fractions from a low value petroleum resid [3]. This process typically operates in the temperature range of 450-500 °C [3]. For the purpose of this research we decided to incorporate coal into a simulated delayed coking process and termed this novel process co-coking. The intent of this novel process was to obtain liquid products that posses coal-derived structures which, when hydrotreated, would produce a product with higher thermal stability than petroleum-based fuels.

The work presented here focuses on the effects of different feed ratios and reaction length effects for various co-coking reactions. This work represents a continuation of previous studies of co-coking [4,5,6,7].

Experimental

Three coals were originally selected based on their high fluidity, high volatile content and relatively low ash values [7]. This paper, however, will focus on an in-depth study of the Powellton seam coal, to determine effects of reaction conditions, such as feed ratio and reaction length. The trends obtained from this particular coal can then be related to the other two coals based on previous research [6,7]. The coal was ground to a -60 mesh and vacuum dried at 110 °C for 2 hours prior to each experiments to remove excess moisture. Two different petroleum resids were employed. The first was a coker feed supplied by BP America. The second was a decant oil supplied by Marathon Oil Company. Both resids were used as received.

These coking reactions were carried out in a constructed vented reactor system. Figure 1 displays a schematic of reactor system utilized. This system consisted of a modified microautoclave reactor (tubing bomb) that was attached to a catchpot system immersed in an ice bath. The reactor system was developed to model aspects of delayed coking in the laboratory. The bomb portion of the system was intended to model a coking drum, while the catchpot was used to catch volatiles, which were then, re-condense into liquids. Before each reaction, the reactants were placed in the bomb portion of the reactor system in various feed ratios. The bomb portion, piping and catchpot were then purged with nitrogen to remove any air within the reactor system and finally left at ambient pressure. The bomb portion of the reactor system was then placed in a fluidized sand bath at a temperature of 465°C, while the

Figure 1: The vented reactor system

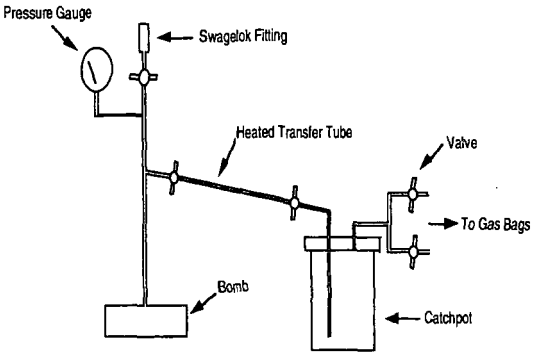

catchpot portion was placed in an ice bath. This temperature proved from previous work [6,7] to produce desirable liquid and solid product yields. Reaction length was varied.

Once the reaction was complete, the reactor system was left to cool. The liquids that accumulated in the catchpot portion of the reactor system were collected and subjected to a hexane extraction to obtain the oil products. The products were then removed from the bomb portion of the reactor system and subjected to a tetrahydrofuran (THF) Soxhlet extraction and finally a hexane extraction to obtain hexane-solubles. The THF-insoluble products were then collected and dried to obtain the coke product on a dry weight basis.

The hexane-soluble fractions from both the catchpot and bomb portion were subject to semi-quantitative analysis using a Shimadzu GC 17A GC-MS, to identify the composition of oils produced, and a HP 5890 II instrument with an FID high temperature simulation distillation GC, to obtain the various boiling cut points. Ultimate analysis and proximate analysis was performed on the coke products using a LECO 600 CHN analyzer and a LECO MAC 400 respectively. Optical microscopy was also performed on the coke products to determine if any interactions were occurring between the coal and petroleum resids.

Results and Discussion

Table 1 shows the overall distribution of the liquid and solid products obtained from co-coking reactions at 465°C for various feed ratios and reaction lengths. We know from previous research that the product distribution from these vented co-coking reactions is unaffected by temperature effects [7]. During the co-coking reactions, partial vaporization and mild thermal cracking, occurs causing both gas and light boiling distillates to flash distillate into the cooled catchpot [8]. The remaining heavy liquids in the bomb portion of the reactor are further subjected to cracking and polymerization reactions, which produce more gas. These gases are also re-condensed in the catchpot [8]. Along with the gases, a solid coke product is formed as a result of cracking reactions. This effect was evident when we examine the product distribution effect versus reaction duration. As the reaction length was increased for a particular feed ratio, the overall liquid yield decreased, while the solid product yield increased. The decrease in overall liquid product yield was mainly a result of the drastic decrease in the THF soluble liquid products as reaction time increased. This occurred because the liquids were exposed to further cracking reactions. The catchpot liquids, however, were unaffected by reaction length, since most of the liquids were flashed off very early in the reaction.

Table 1 also shows the feed ratio effect on the product distribution of co-coking reactions at 465°C. As the amount of petroleum resid was increased in these co-coking reactions for a particular reaction length, the overall liquid products increased, while the overall solid products decreased. Generally the increase in overall liquid product results from an increase in liquid products collected in the catchpot portion of the reactor system. This concurs with logic, since an increase in the amount of paraffinic liquid results in an increase in volatiles, which are easily re-condensed. This present reactor system was not designed to accommodate for adequate gas collection. However, the amount of gas most likely produced from these co-coking reactions, according to mass balances, would be negligible.

The addition of coal from previous studies [6,7] has been shown to decrease the overall liquid product yield when compared to a heat-treated petroleum resid alone. The coal seems to contain highly reactive components that initiate radical reactions that result in retrogressive polymerization reactions.

Overall these liquid and solid yields are comparable to an industrial delayed coking process product distribution of 70% liquids, 10% gas, and 20% coke [3,8]. The product distribution results verify that simplified delayed coking was being simulated by the vented reactor system.

However, our primary goal of this research was to produce low-boiling distillates that can be hydrotreated to produce a thermally stable coal-derived jet fuel. To determine the extent of suitability of the liquid products produced from these co-coking reactions for jet fuel, high temperature simulation distillation GC was performed on the hexane-soluble fractions. For this research, the desired boiling range for the hexane-soluble fraction was 180-330°C. This boiling distribution was defined as the jet fuel range. Figure 2 shows the effect of feed ratio on the liquid yield that fell within the jet fuel boiling range for various co-coking reactions at 465 °C for two hours. The general trend observed was that as more coal was added to these co-coking reactions, the greater the liquid yield, from the catchpot, that distills in the jet fuel boiling range. However, process conditions limit the amount of coal that can be added to a delayed coker. Although the jet fuel boiling yield from the 1:1 ratio of Powellton coal and decant oil in Figure 2 demonstrates a desirable yield of distillates, the ability to process this feed mixture through connective piping in an industrial delayed coker becomes a concern.

Another general trend observed from Figure 2 was that the addition of coal decreases the overall yield of products that distill in the jet fuel boiling range when compared to reaction with heat-treated resid only. The exception that occurred here was with the coker feed. The addition of coal to the coker feed seemed to enhance the yield of jet fuel distillates. This most likely occurred because both the coal and coker feed were acting as hydrogen donors toward the more aromatic components produced in these reactions. This enhancement of the jet fuel boiling distribution yield did not occur when the Powellton coal and decant oil are co-coked, since the decant oil does not appear to act as a hydrogen donor. This explanation was supported by the results obtained when a mixture of the two resids was coked in the presence of the coal. We saw an increase in the yield for the 180-330 °C boiling range when the coker feed was incorporated into the co-coking reactions with decant oil and Powellton coal. The results seem to show that both Powellton coal and the coker feed act as hydrogen donors during these coking reactions, while the decant oil acts as an initiator of radical reactions.

Figure 3 shows the effect of reaction length and feed ratio on the liquid yield from the catchpot that fell within the jet fuel boiling distribution. The general trend observed was that, as reaction length increased, an increase in the jet boiling distribution range occurred. However, an important note was that although the percent yield in the jet fuel range increased as reaction length increased, the overall liquid product being produced decreased. This was mostly likely due to secondary cracking reactions of the heavy liquid, producing more volatiles. Another trend observed involved jet fuel yields from co-coking reactions involving the coker feed, decant oil and the Powellton coal. These yields fell exactly in between the Powellton/coker results and the Powellton/decant results for corresponding reaction lengths and feed ratios.

Ultimate analysis was preformed on the hexane-soluble fractions produced from co-coking reactions at 465°C to determine the quality of products being produced. Table 2 shows the H/C ratio for the hexane-soluble products. The results showed the liquid H/C ratio obtained from reactions with a 1:2 feed ratio (coal:resid) in the catchpot were unaffected by reaction length. These results further indicated the liquids obtained in the catchpot had undergone flash pyrolysis. Table 2 also shows that as the feed ratio was increased to 1:4 (coal:resid) there was no real significant effect in the catchpot H/C ratio. While the liquid H/C ratios from the bomb portion showed a decrease in the H/C ratio as reaction length was increased. This occurred because of further liquid decomposition in the bomb portion of the reactor during longer co-coking reactions. When the feed ratio was increased to 1:4 (coal:resid) a higher bomb H/C ratio occurred as a result of the increased concentration of paraffinic compounds.

Ultimate analysis and optical microscopy were performed on the THF-insoluble products to give an indication of the quality of the coke being produced. Figure 4 illustrates that as reaction length was increased, the H/C ratio of the coke product decreased, indicating a more carbon-rich product. This trend was a result of cracking and polymerization reactions that occur in the co-coking reactions. The effect of feed ratio was negligible on the solid H/C ratio.

Optical microscopy indicated enhancement of coal particles when Powellton coal and decant oil was co-coked. However, when the coke products from the coker feed and Powellton coal were examined, no interactions were observed. Varying the feed ratio had no effect on this reaction matrix. Results from co-coking of the three reactants showed that the influence of the decant oil on the coal particles diminished as compared to the coal and decant oil interaction. The influence of the decant oil in this tri-coking proved to be quite variable throughout the

sample. As a result some coal particles were fully enhanced, and some remained unaffected, but most coal particles fell somewhere in between the two extremes.

Conclusions

From work to date we can adequately conclude that we are upgrading these heavy petroleum resids by producing a coke product that is more carbon and liquids with increased H/C ratios. It was found that by increasing the feed ratio to favor the addition of a petroleum resid, the overall liquid product yield increased, but a decrease in the jet fuel boiling distribution yield was observed. While little effect was observed on the H/C ratio of the liquids obtained when the feed ratio was increased, an increase in reaction length resulted in a decrease of the overall liquid products and an increase in the jet fuel boiling distribution yield. In conclusion this process seems to be simulating the delayed coking process on a laboratory scale.

Acknowledgements

The authors would like to express their gratitude to the Department of Defense and Air Force Wright-Patterson Laboratory for the support under contract F33615-98-D2802 delivery order 6.

References

1. Elliot, M.A.(Ed.), in "Chemistry of Coal Utilization Secondary Supplementary Volume", Wiley-Interscience Publication, New York, (1981).
2. Kural, O.(Ed.), in "Coal: Resources, Properties, Utilization, Pollution", Orhan Kural, Turkey, (1994).
3. Speight, J.G.(Ed.) in "The Chemistry and Technology of Petroleum. 2nd Edition", Marcel Dekker Inc., New York, (1991).
4. Martin, S.C., Tomic, J., and Schobert, H.H., ACS Div. Fuel Chem. **42**, 3, 121, (1997).
5. Badger, M.W., Fickinger, A.E., Martin, S.C., Mitchell, G.D., and Schobert, H.H., AIE 8th Australian Coal Science Conference Preprints p. 245, December 1998
6. Fickinger, A.E., Badger, M.W., Mitchell, G.D., and Schobert, H.H., ACS Div. Fuel Chem. **44**, 1, 106, 1999.
7. Fickinger, A.E., Badger, M.W., Mitchell, G.D., and Schobert, H.H., ACS Div. Fuel Chem. **49**,1,218,1999.
8. DeBiase, R., Elliott, J.D., and Hartnett, T.E., *Petroleum Derived Carbons*, ACS Symposium Series No. 303, 156, 1986.

Table 1: Feed ratio and reaction length effects on product yields from co-coking reactions with Powellton coal and the two petroleum resids at 465 °C

		PRODUCT YIELDS			
		Feed Ratio 1:2		Feed Ratio 1:4	
RESID	TIME	Liquid %	Solid %	Liquid %	Solid %
Coker	30 minutes	83.61	24.78	69.19	26.71
Coker	2 hours	38.84	40.74	61.54	30.98
Coker	4 hours	48.71	38.87	55.78	30.20
Decant	30 minutes	73.09	28.57	78.23	13.78
Decant	2 hours	55.47	37.67	56.88	34.03
Decant	4 hours	39.68	43.12	49.24	49.24
Decant/Coker	30 minutes	53.86	30.50	•	•
Decant/Coker	2 hours	44.64	39.88	60.59	26.50
Decant/Coker	4 hours	52.97	40.49	62.01	26.53

• Data Missing

Table 2: Feed ratio and reaction length effects on hexane-soluble product H/C ratios from co-coking reactions with Powellton coal and various petroleum resids at 465 °C

			HEXANE SOLUBLE H/C RATIOS			
			Feed Ratio (1:2)		Feed Ratio (1:4)	
COAL	RESID	TIME	CATCHPOT	BOMB	CATCHPOT	BOMB
Powellton	Coker	30 minutes	2.30	1.64	2.49	2.01
Powellton	Coker	2 hours	1.86	1.36	2.30	1.36
Powellton	Coker	4 hours	2.30	0.87	2.47	1.03
Powellton	Decant	30 minutes	1.30	1.05	1.23	0.90
Powellton	Decant	2 hours	1.40	0.70	1.45	0.82
Powellton	Decant	4 hours	*	0.90	1.59	0.76
Powellton	Decant/Coker	30 minutes	1.60	0.98	*	*
Powellton	Decant/Coker	2 hours	1.51	1.16	1.74	1.46
Powellton	Decant/Coker	4 hours	1.67	1.82	1.78	1.04

* Data missing

Figure 2: Feed ratio effects on the jet fuel boiling distribution (180-330°C) for the hexane-soluble fractions from co-coking reactions at 465°C for two hours

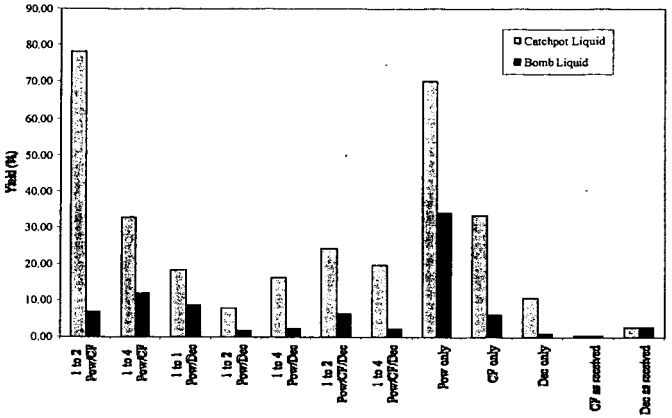

Figure 3: Reaction Length effects and feed ratio effects on the jet fuel boiling distribution of the catchpot hexane-soluble fraction from co-coking experiments at 465 °C.

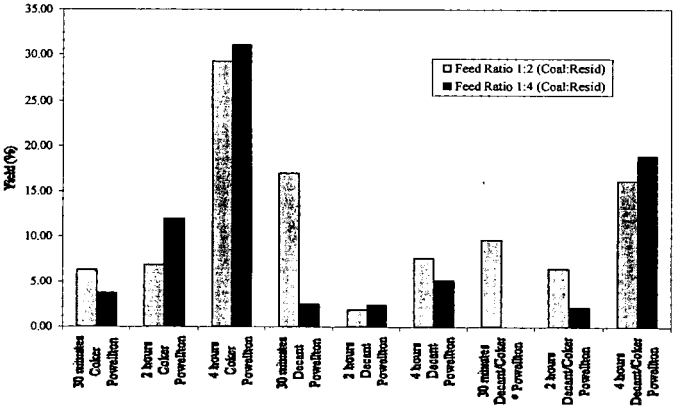

Figure 4: Reaction length and feed ratio effects on the solid coke products formed from co-coking reactions at 465 °C with Powellton coal and the two petroleum resids

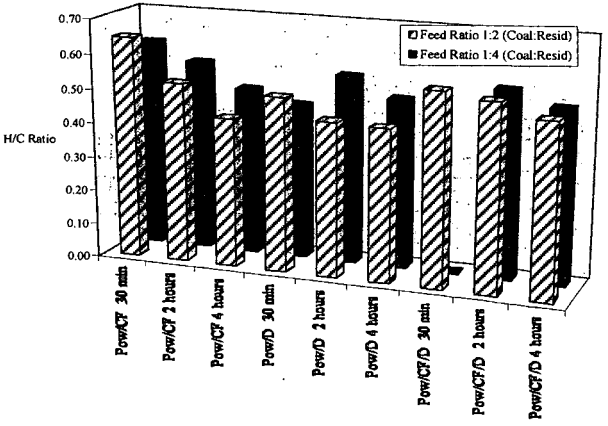

COMPARISON OF THE THERMAL STABILITY OF COAL-DERIVED JET FUELS IN THE AUTOXIDATIVE AND PYROLYTIC REGIMES UNDER BATCH AND FLOW CONDITIONS

John M. Andrésen, James J. Strohm and Chunshan Song*
Applied Catalysis in Energy Laboratory, The Energy Institute
The Pennsylvania State University, University Park, PA 16802

KEYWORDS: Pyrolysis, thermal stability, aviation jet fuels.

ABSTRACT

The thermal stability of coal- and petroleum-derived jet fuels and the associated model compounds decahydronaphthalene and n-tetradecane, as they go through the autoxidative and pyrolytic regime both under batch and flow conditions, was studied. Under batch reactor conditions, the decahydronaphthalene showed excellent thermal stability up to 500°C, whereas the n-tetradecane started its cracking process at around 450°C. Flow reactor studies mirrored the thermal decomposition of the model compounds, although the cracking appeared at higher bulk fuel temperatures. The thermal behavior of the experimental jet fuels also confirmed that the paraffinic proportion of the fuels is the main reason for thermal fuel degradation.

INTRODUCTION

Cycloalkane-rich liquids, such as those derived from coal, have great potential as precursors for advanced jet fuels that meet the more stringent thermal stability requirements for the future high-Mach jet aircraft [1]. Currently, commercial planes are utilizing conventional paraffinic based jet fuels that may be exposed to temperatures up to 300°C [2]. However, as the flight speed will be increased to high Mach numbers, the fuel is expected to experience temperatures as high as 482°C (900°F) or above, since the jet fuel also functions as the main coolant for the different electronic and mechanical parts of the aircraft. Even though the residence time at such elevated temperatures is expected to be fairly short (matter of minutes or less), the jet fuels presently used have been shown to form solid deposit that can lead to catastrophic malfunction of the jet aircraft. The current jet fuels are petroleum-derived and consequently rich in linear alkanes, which are highly susceptible to pyrolytic cracking, resulting in coking [3]. The thermal stability of a jet fuel in the pyrolytic regime can be greatly enhanced by utilizing liquids rich in cyclo-alkanes [4]. This is the case for hydrotreated coal-derived liquids, where the aromatic structures have been transformed over to their corresponding cyclo-alkanes [5]. An additional problem with jet fuels is the presence of dissolved oxygen from air, which reacts with the fuel during the autoxidative regime (150-250°C) before the fuel and its oxygenated reaction products enter the pyrolytic regime (400-500°C) [6]. Accordingly, the present study compares the thermal stability of coal- and petroleum-derived jet fuels and associated model compounds, as they go through the autoxidative and pyrolytic regime, both under batch and flow conditions. Differences in chemical reactivity between linear- and cyclo-alkane model compounds are related to the superior thermal stability of the coal-derived jet-fuels.

EXPERIMENTAL

The samples investigated were the two model compounds tetradecane (TD, Aldrich 99%) and decahydronaphthalene (DHN, Aldrich 98%, a mixture of cis- and trans-decahydronaphthalene), a hydro-treated light cycle oil (DA/HT LCO) and a coal-derived jet fuel named JP8C.

For the batch study, a volume of 5 ml was charged into a microautoclave with a total volume of 25 ml [7]. The system was pressurized with 100 psi of air and heated in a fluidized sandbath. The heating-rate used was approximately 5°C min^{-1} from room temperature and the microautoclaves were removed upon reaching 250, 350, 450 and 500°C. After reaction, the microautoclaves were rinsed of sand and quenched. When the microautoclaves were cooled to ambient temperature, the gas phase and liquid fraction were removed for analysis. The tube and the stem of the microautoclave were washed in pentane until a clear color was obtained and then dried. The amount of solid deposition was determined from the increase in weight of the tube and stem.

The GC-MS analysis of the liquid products was performed on a Shimadzu GC-174 coupled with a Shimadzu QP-5000 MS detector. The column used was a Restek XTI5 column with a coating phase of 5% diphenyl / 95% dimehyl polysiloxane and it was heated from 40 to 290°C with a heating rate of 6°C min^{-1}.

The flow reactor is outlined in Figure 1. The fuel tank was degassed with high-purity N_2 (99.9%) to ensure the absence of oxygen for the pyrolytic study. In addition, the jet fuel was purged with air to compare our autoxidative studies in batch reactors with those of the flow reactor. An HPLC pump was used to pressurize the jet fuel up to 700 psi with a flow rate of 6 ml/min. Within the furnace, a 0.040" (1.02 mm) ID silcosteel tubing was used. This ensured a liquid hourly space velocity (LHSV) of 450. The temperature profile was established by welding thermocouples to the tubing in addition to inserting thermocouples within the tubing and at the

exit of the furnace (the last thermocouple is indicated in Figure 1, where also a silcosteel union tee was used to minimize catalytic jet fuel degradation). The temperature profile is shown in Figure 2 and is somewhat different to that reported in the literature for other flow reactor systems [8]. The GC/MS traces are reported according to the exit temperature of the actual fuel. Immediately after exiting the furnace, the jet fuel is cooled by refrigerated ethylene glycol. The tubing used is also silcosteel to avoid secondary reactions during cooling of the stressed jet fuel. The cooled jet fuel is then filtered to accumulate any solids formed using a 0.8 μm filter. Further, a back pressure valve is used to control the furnace pressure. The cooled jet fuel is then allowed to enter a storage vessel, where the liquid products are separated from the gaseous products.

RESULTS AND DISCUSSION

Batch reactor studies The content of the liquid remaining for n-tetradecane (TD), decahydronaphthalene (DHN) and the coal-derived jet fuel JP8C stressed under the influence of air in the temperature range 250 to 500°C is compared in Figure 3. At low temperatures (250 - 350°C), the formation of gas and solid products is very small. However, as the temperature is increased to 450°C and indeed for the one stressed at 500°C, the content of liquid remaining is reduced. Especially the linear alkane, TD, has a drastic lowering of the liquid phase, reaching a level below 80%. The coal-derived jet-fuel, JP8C, shows an improved thermal stability compared to TD, where above 90% of the liquid remains, while the cycloalkane, DHN, shows the highest ability to resist thermal cracking. The reduction in the liquid produces gas and solids, and although not shown here the linear alkane forms about 0.2 wt% solid residue already at 250°C. The solid deposition is not significantly increased at 350°C, but rises sharply when stressed further to 500°C, following a similar trend to the solid deposition found using flow-reactor studies [8, 9]. The vast difference in liquid yields between liquids rich in linear alkane and those mainly containing cyclo-alkane (including the JP8C and LCO HT/DA) as showed in Figure 2, can be explained further by studying the ability of the different hydrocarbons to resist thermal cracking. Figure 4 shows the variation in the remaining concentration of TD and DHN in the liquid products with temperature, taking into account the formation of gas and solids. In the autoxidative zone the reduction in the concentration of the two compounds is small. However, as the temperature reaches the pyrolytic regime, a great difference in thermal stability of the two compounds is shown. At 500°C only around 35% TD is remaining, while 85% of the DHN has not reacted.

The above differences in thermal stability can be related to the differences in the oxidation chemistry in the autoxidative zone and the thermal stability of the oxygenated compounds from linear- and cyclo-alkanes to remain in the liquid. Figure 5 shows the GC/MS trace of the reaction products from stressing of TD in air up to 250°C. A range of linear alkane products is present as the tallest peaks in the different peak clusters. A row of compounds with oxygen functional groups is associated with each linear alkane, such as acids, aldehydes and ketones. The compounds present at 250°C do not alter when stressed up to 350°C, but a drastic change in the product distribution appears as the temperature is increased to 450°C. At this temperature the concentration of n-alkanes are greatly increased and also 1-alkenes are produced as a result of thermal cracking [10]. Although, some oxygenated compounds still remain in solution, the reactivity of these species clearly adds to the thermal degradation of the linear alkane, TD. The cyclo-alkane, DHN, also experiences some oxidation in the autoxidative zone, as shown in Figure 6. The mixture of trans- and cis-decahydronaphthalene used here (retention time of 14 and 15 minutes, respectively), gave oxygenated products which appear in a narrow retention time range of 18 to 21 minutes. Particularly ketones and alcohols dominate, where compounds such as 2-butyl cyclohexanone and decahydronaphthol are abundant. The presence of alcohols in the products from DHN indicates that oxygenated cyclo-alkane compounds are more stable than their linear equivalents. As the temperature is increased to 450°C only small changes in the product distribution occur, which again confirm the higher stability of cyclo-alkanes derived compounds, where oxygen is captured. By further increasing the stressing up to 500°C, non-oxygenated single ring compounds, such as 1-methyl cyclohexene, appear at lower retention times, but still the oxygenated compounds are present. The development of the hydrogen-donor tetrahydronaphthalene may also further enhance the thermal stability of the liquid.

The changes in the product distribution from the coal derived jet fuel, JP8C, stressed under air at 250 and 500°C are shown by the GC/MS traces in Figure 7. At 250°C, JP8C is rich in one and two ring cyclo-alkanes, and at longer retention times a series of long-chain linear alkanes in the range of C12 to C18 is present. When stressed up to 500°C, only small changes in the cyclo-alkane distribution occur, while the concentration of the linear alkanes has decreased drastically. Based on the study of stressing TD in both the autoxidative zone and further in the pyrolytic regime, the reduction in the linear alkane concentration can be due to the following two reasons. Firstly, the tendency of linear alkanes to react with oxygen and form less stable compounds, and secondly, the lower thermal stability of the linear alkanes themselves in comparison to cyclo-alkanes.

Flow reactor studies The findings from the batch reactor studies were further correlated with stressing of model compounds under flow conditions both in the absence and presence of oxygen. Silcosteel tubing was used in this work to minimize any metal surface-catalyzed fuel decomposition. Figure 8 shows the concentration of DHN remaining as a function of the exit temperature of the liquid. With a LHSV of 450, DHN presents a similar behavior when stressed under both N_2 and air, where the thermal cracking of the liquid takes place at temperatures above 620°C. Indeed, nearly identical evaluation of the DHN both under N_2 and air supports the findings from the batch reactor studies that the air uptake by DHN is reduced in comparison to linear alkanes such as TD. Flow reactor studies using TD were also carried out. However, the TD generated extensive coke formation resulting in blockage of the 1/16" tubing through the furnace. This was observed under both N_2 and air, where the dotted vertical line in Figure 8 shows the temperature at which the TD under oxidative conditions started coking, while the solid line indicates the same temperature for TD under inert atmosphere. The fact that TD actually cokes at temperatures where DHN is essential unconverted again supports the previous findings from the batch reactor studies. The difference in the thermal stability of cyclo-alkanes and linear alkanes is also illustrated in Figure 9, showing the GC/MS traces of the LCO derived jet fuel, DA/HT LCO, stressed alone with fuel outlet temperatures of 520 and 620°C. With a LHSV of 450 very little jet fuel degradation takes place when the maximum fuel outlet temperature was 520°C, and the GC/MS trace is virtually identical to those reported on the initial DA/HT LCO fuel [3, 5]. Increasing the temperature to 570 and 590°C (not shown here) there is some pyrolytic cracking of the jet fuel, but it is not before 620°C that the appearance of aromatic compounds starts becoming significant. This scenario is somewhat different to that of the batch reactor studies, where similar changes were observed at a lower temperature for the coal derived jet fuel JP8C (Figure 7). On the other hand, during the batch reactor studies the jet fuel had residence times substantial longer than that of the present flow reactor experiments. However, again there are only slight changes in the cyclo-alkane compounds, and as expected the thermal exposure at 620°C has cracked virtually all the long chain alkanes into lighter compounds and aromatic compounds, opening the possibility for detrimental solid deposition.

CONCLUSIONS

The changes in product distribution for a linear alkane, n-tetradecane (TD), and a bicyclic alkane, decahydronaphthalene (DHN) were related to a cycloalkane-rich coal-derived jet fuel, JP8C, in batch reactors and a light cycle oil-derived jet fuel, DA/HT LCO, under flow conditions. Under batch conditions, the linear TD showed less thermal stability than that of JP8C, and particularly lower than that of DHN when stressed under air. This was associated with the formation of a range of oxygenated compounds from TD such as acids, aldehydes and ketones, which showed lower thermal stability than those oxygenated compounds derived from DHN. The flow reactor studies confirmed the findings under batch conditions, but the temperatures at which cracking occurs were shifted to considerably higher temperatures.

ACKNOWLEDGEMENTS

The authors wish to thank the US Air Force Wright Laboratory and the US AFOSR for their support. We are grateful to Prof. Harold H. Schobert of The Pennsylvania State University for his support and discussions, and to Mr. William Harrison III, Dr. Tim Edwards and Dr. Cindy Obringer of WPAFB for helpful suggestions.

REFERENCES

(1) Edwards, T., Prep. Am. Chem. Soc.-Div. Petr. Chem., 41(2), 481-487 (1996).
(2) Yoon, E.M., Selvaraj, L., Song, C., Stallman, J.B and Coleman, M.M., Energy & Fuels, 10, 806-811 (1996).
(3) Andrésen, J.M., Strohm, J.J. and Song, C, Prep. Am. Chem. Soc.-Div. Petro. Chem., 43(3), 412-414 (1998).
(4) Andrésen, J.M., Strohm, J.J. and Song, C, Prep. Am. Chem. Soc.-Div. Fuel Chem., 44(1), 199-203 (1999).
(5) Strohm, J.J., Andrésen, J.M. and Song, C, Prep. Am. Chem. Soc.-Div. Petro. Chem., 44 (3), 386-390 (1999).
(6) Hazlett, R.N., Thermal Oxidative Stability of Aviation Turbine Fuels, ASTM, Philadelphia, PA (1991).
(7) Song, C., Eser, S., Schobert, H.H. and Hatcher, P.G., Energy & Fuels, 7, 234-243 (1993).
(8) Minus, D.K. and Corporan, E., Prep. Am. Chem. Soc.-Div. Petro. Chem., 43(3), 360-363 (1998).
(9) Edwards, T. and Atria, J.V., Prep. Am. Chem. Soc.-Div. Petro. Chem., 40(4), 649-654 (1995).
(10) Andrésen, J.M., Strohm, J.J. and Song, C, Prep. Am. Chem. Soc.-Div. Fuel Chem., 44(1), 194-198 (1999).

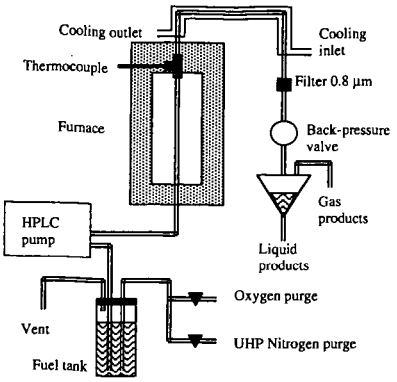

Figure 1. Outline of flow reactor.

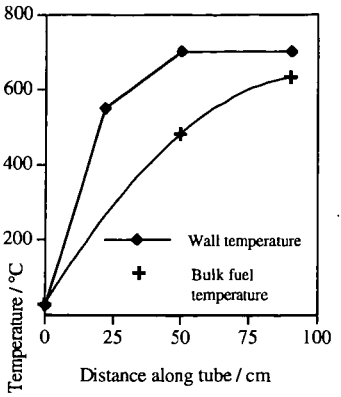

Figure 2. Temperature profile of the flow reactor system, showing correlation between wall and actual bulk fuel temperatures.

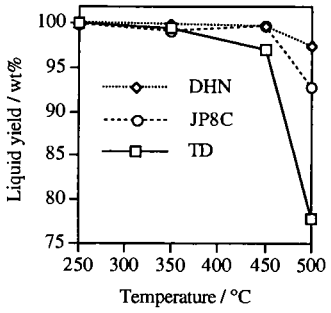

Figure 3. Comparison of liquid remaining for TD, DHN and the coal-derived jet fuel JP8C stressed in batch reactor under the influence of air in the temperature range 250 to 500°C.

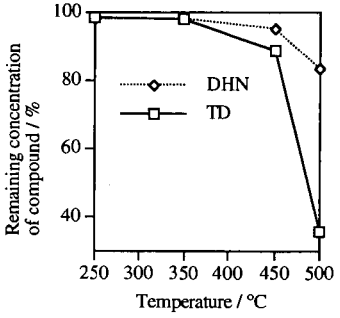

Figure 4. Variation in the remaining concentration of tetradecane and decahydronaphthalene with temperature stressed under 100 psi air in batch reactor.

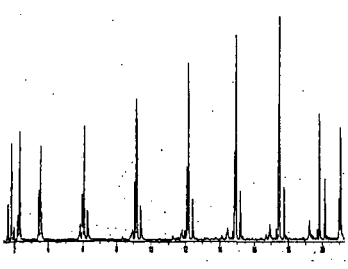

Figure 5. GC/MS trace of the reaction products from stressing TD in batch reactor under 100 psi air up to 250°C.

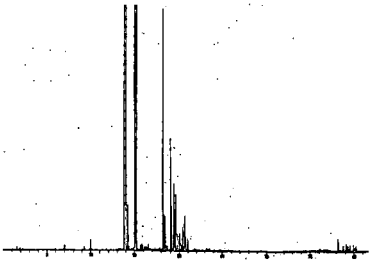

Figure 6. GC/MS trace of the reaction products from stressing DHN in batch reactor under 100 psi air up to 250°C.

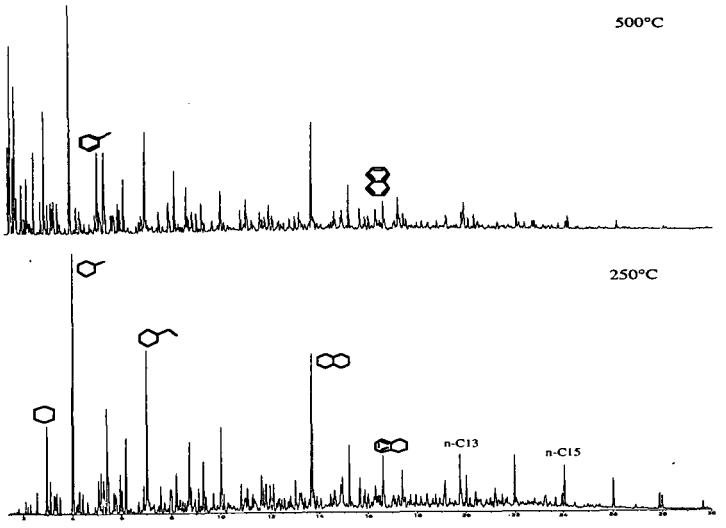

Figure 7. GC/MS traces of the coal derived jet fuel, JP8C, stressed under 100 psi air in batch reactors from room temperature to 250°C (bottom) and 500°C (top).

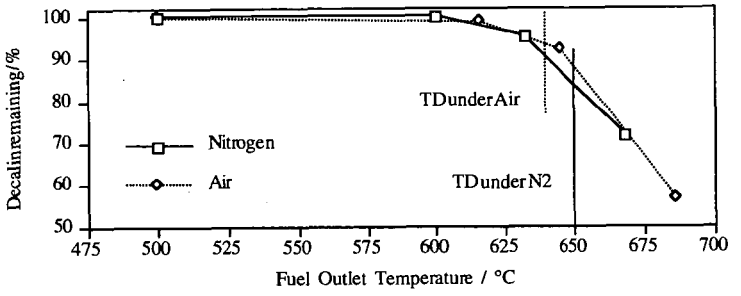

Figure 8. Remaining concentration of DHN with temperature under flow conditions.

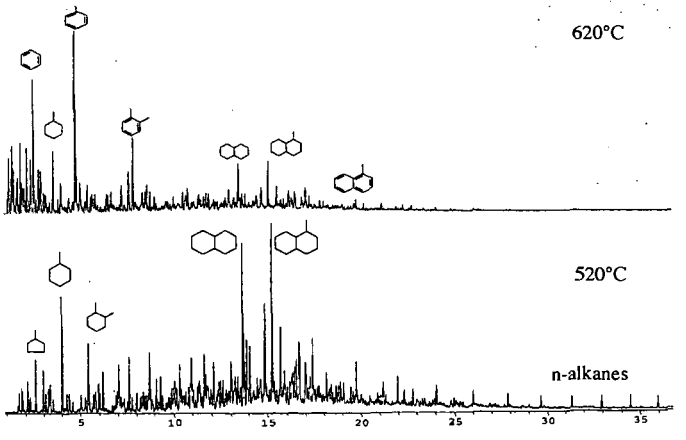

Figure 9. GC/MS traces of the DA/HT LCO jet fuel under flow conditions at fuel outlet temperatures of 520 and 620°C.